MASTER THESIS

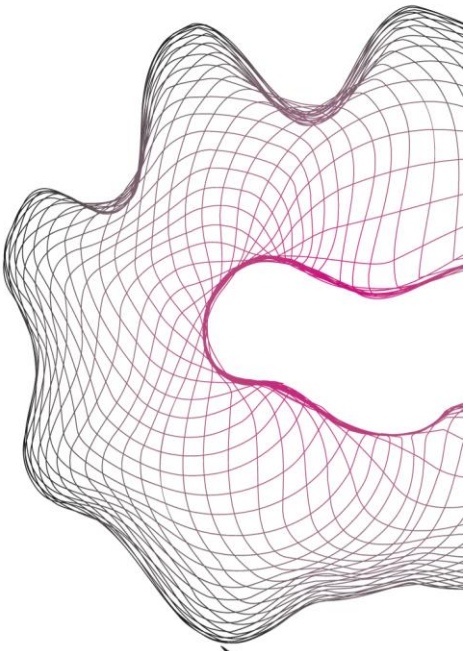

DESIGN AND CONSTRUCTION OF A SETUP THAT REPRESENTS THE BEHAVIOR OF A HELICOPTER ROTOR BLADE SYSTEM

J. Wolters

FACULTY OF ENGINEERING TECHNOLOGY
APPLIED MECHANICS

EXAMINATION COMMITTEE
prof.dr.ir. A. de Boer
dr.ir. R. Loendersloot
dr.ir. W.B.J. Hakvoort

DOCUMENT NUMBER
CTW.14/TM - 5741

UNIVERSITY OF TWENTE.

14-11-2014

MASTER THESIS

DESIGN AND CONSTRUCTION OF A SETUP THAT REPRESENTS THE BEHAVIOR OF A HELICOPTER ROTOR BLADE SYSTEM

Student

Full name Joris Wolters

Student number s0166847

University

Institution University of Twente

Faculty Engineering Technology

Research group Applied Mechanics

Chair Structural Dynamics & Acoustics

Supervisors dr.ir. R. Loendersloot and A. Sanchez Ramirez MSc.

Graduation professor prof.dr.ir. A. de Boer

City and country Enschede, The Netherlands

UNIVERSITY OF TWENTE.

Preface

This report presents the work that has been performed during my master's assignment. This assignment was done at the department of Applied mechanics at the University of Twente. For this assignment, I designed and built a demonstrator that represents the behavior of a helicopter Rotor Blade System. It has been a memorable year with several ups and downs during the assignment. With finishing this assignment, my career as a Mechanical Engineering student also comes to an end. Looking back on my life as a student, I can conclude that it has been an amazing time and that I've had lots of unforgettable experiences during my student life. Leaving my parent's house to live in Enschede, the many group projects during the bachelor's phase and the study tour to Dubai and Indonesia in 2010 are some of the highlights of the bachelor phase. For my master phase, my internship at KND in Cape Town in 2013 has been an absolute highlight. It really opened my eyes for the possibility of working abroad and besides that, it was a wonderful time in an amazing city and country.

I would like to thank some people for being any kind of help during this assignment. First of all, I would like to thank my supervisor Andrea for the very involved supervision I received from her throughout this whole assignment. Many thanks also goes out to my other supervisor Richard, for the good supervision, for reading and correcting the report several times and for keeping the right amount of pressure on finishing the report. Furthermore, I would like to thank André for looking at the problems from a different angle and showing me other possible solutions during the discussions we had throughout this assignment. Thanks to Dannis for giving me tips on the design of the flexure mechanism. For discussing the design and showing what's possible in the workshop and what's not, I would like to thank Norbert. Many thanks also goes out to the rest of the people who helped me with making the parts for the demonstrator at the workshop; Martin, Joop, Arjan, Leo, Theo and Peter. I'd like to thank Axel for his help with performing the tests with the demonstrator. For taking the time to read my report and to give advice, lots of thanks and appreciation go out to my sister Rinske and my friends Jesper and Rogier. Then I would like to thank all the people who I worked with in room N242, for the interesting discussions we had during the many coffee breaks and for the pleasant climate and ambiance in which we worked. Thanks to my friends and family who have been of any kind of moral support throughout this last year; for not asking about the thesis when I wanted to keep my mind off things and for willing to listen and give advice when I was struggling with the assignment. Last but not least, I would like to thank my parents for the financial and moral support that I received throughout my study.

Summary

Rotor Blade Systems (RBS) like helicopters or wind turbines are complex mechanical structures that make use of flexible rotating blades to fulfill their functions. When an RBS is in operation, the blades will display several types of deformations that are highly dependent on the flight (helicopter) or weather (wind turbine) conditions. With the rotor and blades usually being the main source of vibrations in RBS, it would be favorable to monitor the behavior of the system by monitoring directly on the rotor and blades. On-blade monitoring is however not that advanced in RBS.

Previous performed experimental research regarding RBS was reviewed to investigate the added value of on-blade monitoring in systems like these. The reviewed experiments are presented in a table that shortly describes the characteristics and the goals of the experiments. Furthermore, each of the experiments was classified on the basis of the number of Degrees Of Freedom (DOFs) that were being excited and monitored. It turned out that not a lot of experimental research was performed where multiple DOFs were being excited and monitored.

This thesis focuses on the design and construction of a functional setup that represents the behavior of a helicopter RBS. This demonstrator can be used to test different strategies for on-blade monitoring in RBS. Investigation of the characteristics of RBS learned that the behavior of these systems is complex. Therefore, the complexity of the behavior is reduced for the design of the demonstrator. How this complexity was reduced is described after defining the behavior of the RBS. On the basis of the desired behavior of the demonstrator, the design requirements are stated. An important requirement was that the ratio between first mode frequencies of the setup correspond with those of a real helicopter. Another important requirement was that the demonstrator could be used to test different blade profiles on it.

The demonstrator that was eventually built contains of a single hanging, for which cyclic pitch (change of the blade angle over the radial axis) and flap (up and down movement of the blade) are excited. By exciting two DOFs, the demonstrator can potentially fill a gap in the table with the classified experiments; i.e. by exciting and monitoring multiple DOFs. Cyclic pitch is actuated at constant frequency by a Voice Coil Motor (VCM), while flap is actuated with a broadband frequency signal by a shaker. Furthermore, the demonstrator contains hinges for all DOFs. The flap and lag hinges have a rotational stiffness, generated by torsion springs that are connected on the outer side of the hinges. These rotational stiffnesses in the hinges are needed to be able to realize the required mode frequencies. By keeping the torsion springs outside the hinges, it is possible to replace the springs if other stiffnesses are required when different blade profiles are tested.

After the design was made and approved, the parts were manufactured and ordered and the total system was assembled. With this assembled demonstrator, different tests were performed to validate if it fulfills the design requirements that were stated. It occurred that the amount of play in the system was too much to be able to determine the different blade mode frequencies directly out of the demonstrator. For this reason, the blade and the flap hinge were tested individually to determine the flapping mode frequencies. It appeared that the measured blade frequencies did not exactly correspond with those that were desired by the design requirements, they were however in the right range. Besides performing tests to determine the mode frequencies, the double actuation was tested, i.e. excitation of both pitch and flap. Actuation of pitch by a VCM turned out to be a struggle, due to the magnetic core of the actuator, which made it impossible to find a stable neutral position for it. Besides, due to the fact that the two parts of the VCM make contact at every cycle, actuation of pitch with a VCM introduces unwanted

vibrations in the system, which is highly unfavorable when on-blade monitoring strategies will be tested with the demonstrator.

It was concluded that the demonstrator that was built did fulfill many of the design requirements, but some important recommendations are given to improve the demonstrator. Due to the amount of play, it is not possible to test and monitor the fully assembled demonstrator yet. It is recommended to redesign some of the parts to reduce the amount of play. Furthermore, a different actuator for pitch was recommended to improve the control of the actuation of pitch and to eliminate the unwanted vibrations that come with the VCM. If the recommendations are satisfied, the demonstrator can potentially be used for experimental research on RBS that makes use of both actuation and excitation

Samenvatting

Rotor-blad-systemen (RBS), zoals bijvoorbeeld helikopters of windturbines, zijn complexe mechanische systemen die gebruik maken van flexibele roterende bladen om aan hun functie te voldoen. Wanneer een RBS in operatie is, zullen de bladen verschillende vervormingen laten zien, welke afhankelijk zijn van het type vlucht (helikopter) of het weer (windturbine). Gezien het feit dat de rotor en de bladen vaak de hoofdoorzaak van trillingen in RBS zijn, zou het gewenst zijn om het gedrag van de rotor en de bladen direct te kunnen observeren door het uitvoeren van metingen op het blad en rotor. Het blijkt echter dat het direct op het blad monitoren van RBS nog niet erg geavanceerd is.

Experimenten die met RBS te maken hebben zijn bekeken om de mogelijk toegevoegde waarde van het direct op het blad monitoren in RBS te onderzoeken. De onderzochte experimenten zijn in een tabel weergegeven waarin elk van de onderzoeken kort wordt beschreven middels de eigenschappen en het hoofddoel van de experimenten. Verder zijn de experimenten ingedeeld op basis van het aantal vrijheidsgraden (Degrees Of Freedom, DOFs) welke zijn gemonitord en welke zijn geëxciteerd. Het bleek dat er weinig experimenteel onderzoek gedaan is waarin meerdere DOFs zijn geëxciteerd en gemonitord.

Dit proefschrift richt zich op het ontwerpen en het bouwen van een opstelling welke het gedrag van een helikopter RBS representeert. Deze opstelling kan worden gebruikt om verschillende meetstrategieën voor RBS te testen waarbij er direct op het blad gemonitord wordt. Het blijkt dat het gedrag van RBS complex is, waardoor is besloten om de complexiteit van het gedrag te reduceren voor het ontwerp van de opstelling. In welke mate de complexiteit is gereduceerd zal worden beschreven nadat het gedrag van de RBS is beschreven. Aan de hand van het gewenste gedrag voor de opstelling is een lijst van ontwerpeisen samengesteld. Een belangrijke eis was dat de verhouding tussen de frequenties behorende bij de eerste trillingsvormen van de opstelling gelijk moest zijn aan die van een helikopter. Een andere belangrijke eis was dat de opstelling gebruikt moet kunnen worden om er verschillende bladprofielen mee te testen.

De opstelling die uiteindelijk gebouwd is bestaat uit een hangend blad, waarvoor cyclische pitch (hoekverandering van het blade over de radiale as) en flap (op- en neergaande beweging van het blad) geëxciteerd kunnen worden. Door twee verschillende DOFs aan te sturen, zou de opstelling in potentie een leeg plekje in de tabel met de ingedeelde experimenten kunnen opvullen; namelijk door meerdere DOFs te exciteren en te monitoren. Cyclische pitch wordt met constante frequentie aangestuurd door een Voice Coil Motor (VCM), terwijl flap met een breedband frequentiesignaal wordt aangestuurd door een shaker. Verder heeft de opstelling scharnieren voor alle DOFs. Van deze scharnieren hebben de flap- en lagscharnieren een rotatiestijfheid, die nodig is om de gewenste frequenties bij de trillingsvormen te realiseren. Deze rotatiestijfheden worden gerealiseerd door torsieveren die aan de buitenkant van de scharnieren aan het systeem worden verbonden. Door ze aan de buitenkant te verbinden, wordt de mogelijkheid om de veren te vervangen opengehouden. Dit zou nodig kunnen zijn als andere stijfheden gewenst zijn wanneer andere bladprofielen gebruikt worden.

Nadat de opstelling ontworpen en goedgekeurd was, zijn de verschillende onderdelen gemaakt en besteld en is het hele systeem geassembleerd. Met de opstelling zijn vervolgens testen uitgevoerd om te verifiëren of het aan de eisen voldoet die waren opgesteld. Het bleek dat er te veel speling zat in het systeem om de frequenties behorende bij de trillingsvormen direct uit de opstelling te kunnen bepalen. Om deze reden is er besloten om het blad en het flapscharnier apart te testen, om de frequenties van flap te bepalen. Deze frequenties bleken niet exact overeen te komen met de gewenste frequenties, hoewel ze wel in de buurt van de gewenste waardes zaten. Behalve het bepalen van de frequenties, is de dubbele excitatie

ook getest; het aansturen van zowel pitch als flap. Excitatie van pitch door middel van een VCM bleek een aantal problemen op te leveren. Zo was het door de magnetische kern van de actuator onmogelijk om een stabiele evenwichtspositie te vinden. Daarnaast maakten de kern en de spoel contact met elkaar bij elke cyclus, wat ongewenste trillingen in het systeem met zich meebrengt. Dit is zeer ongewenst wanneer er direct op het blad gemeten moet worden.

Uiteindelijk is er geconcludeerd dat de opstelling die gebouwd is aan veel van de opgestelde eisen voldoet, er zijn echter een aantal belangrijke aanbevelingen gedaan welke de opstelling zouden kunnen verbeteren. Vanwege de hoeveelheid speling in het systeem is het nog niet mogelijk om testen met de volledig geassembleerde opstelling uit te voeren. Om de speling te verminderen wordt er aangeraden om een aantal onderdelen opnieuw te ontwerpen en te bouwen. Verder wordt er geadviseerd om een andere actuator voor de aansturing van pitch te selecteren. Zo kunnen de ongewenste trillingen ten gevolge van de VCM uit het systeem verwijderd worden als pitch wordt aangestuurd. Wanneer er aan de aanbevelingen zal worden voldaan, kan de opstelling in potentie gebruikt worden voor experimenteel onderzoek in RBS waar meerdere DOFs worden geëxciteerd en gemonitord.

Nomenclature

This section a list of terms, abbreviations and symbols that are used throughout this report.

Glossary

Accelerometers are sensors that were used during the testing phase fo this assignment and that can measure the acceleration of the point it is subjected to.
ANSYS is a finite element analysis package that is used during the design process.
Demonstrator is the setup that was designed built during this assignment.
Feathering is the twist motion of the blade around the radial axis.
Flapping is the up and down movement of the blade.
Flexure is the flexible element that is used for the actuation of flap in the demonstrator.
Lead-lagging is the forwards and backwards movement of the blade in the plane of rotation. Lead-lagging is referred to as lagging throughout most of the report.
MATLAB is a technical computing language that is used for the calculations throughout this assignment.
Pitch is the rigid twist of the blade around the radial axis.
Shaker is an actuator that is used to excite the flapping movement in the demonstrator.
SolidWorks is a 3D CAD software package that is used to model the design of the demonstrator.

Abbreviations

DOF stands for Degree Of Freedom
EDM stands for Electric Discharge Machining
FBS stands for Function-Behavior-Structure
FRF stands for Frequency Response Function
RBS stands for Rotor Blade System
RMS stands for Root Mean Square
VCM stands for Voice Coile Motor
WSN stands for Wireless Sensor Networks

List of symbols

$\boldsymbol{A}$	is a constant for the calculation of the natural bending frequency of a beam.
$\boldsymbol{A_{1,2}}$	are the integration constants in the solution for $T(t)$.
$\boldsymbol{A_C}$	is the constant for the calculation of the natural bending frequency of a clamped beam.
$\boldsymbol{A_H}$	is the constant for the calculation of the natural bending frequency of a hinged beam.

$\boldsymbol{B_{1,2,3,4}}$	are the integration constants in the solution for $Y(x)$.
$\boldsymbol{C_f}$	is the desired rotational stiffness of the flap hinge.
$\boldsymbol{C_g}$	is the gravitational rotational stiffness of a pendulum.
$\boldsymbol{C_F}$	is the desired rotational stiffness of the flap hinge.
$\boldsymbol{C_L}$	is the desired rotational stiffness of the lag hinge.
$\boldsymbol{C_{S_F}}$	is the torsional stiffness of the torsion spring that is used for the flap hinge.
$\boldsymbol{C_{S_L}}$	is the torsional stiffness of the torsion spring that is used for the lag hinge.
$\boldsymbol{E}$	is the Young's modulus.
$\boldsymbol{f}$	is the rigid body pendulum frequency of a hanging blade.
$\boldsymbol{f(x,t)}$	represents the external forces on a beam at position x and time t.
$\boldsymbol{f_{f_{el,1}}}$	is the first elastic flapping frequency of the blade.
$\boldsymbol{f_{f_r}}$	is the rigid body flapping frequency of the blade.
$\boldsymbol{f_{l_r}}$	is the rigid body lagging frequency of the blade.
$\boldsymbol{F}$	is the force that the torsion spring legs exert on the demonstrator.
$\boldsymbol{F_{max}}$	is the maximum force that is needed for the actuation of pitch.
$\boldsymbol{F_{RMS}}$	is the root mean square of the force for the actuation of pitch.
$\boldsymbol{g}$	is the gravitational constant.
$\boldsymbol{h}$	is a design parameter of the flexure; it represents the leaf height.
$\boldsymbol{dh}$	is the change in distance between the torsion spring legs.
$\boldsymbol{H}$	is a design parameter of the flexure; it represents the beam height.
$\boldsymbol{H}$	is a characteristic of a cross hinge; it represents half the hinge height.
$\boldsymbol{I(x)}$	is the area moment of inertia of a cross section at position x.
$\boldsymbol{I_{RMS}}$	is the root mean square of the current for the actuation of pitch.
$\boldsymbol{I_y}$	is the mass moment of inertia with respect to the pitch axis of the demonstrator.
$\boldsymbol{K}$	is the rotational stiffness of a cross hinge.
$\boldsymbol{K}$	is the rotational stiffness that is used for the derivation of the effect of such a stiffness on the bending frequency.
$\boldsymbol{K_f}$	is the force constant of the VCM.
$\boldsymbol{K_{flap}}$	is the rotational stiffness of the flap hinge.
$\boldsymbol{K_h}$	is the rotational stiffness of a single hinge of the flexure.
$\boldsymbol{K_{lag}}$	is the rotational stiffness of the lag hinge.
$\boldsymbol{l}$	is a design parameter of the flexure; it represents the hinge length.
$\boldsymbol{l}$	is a characteristic of a cross hinge; it represents the leaf length of a single leaf.
$\boldsymbol{L}$	is the blade length.
$\boldsymbol{L_F}$	is the arm that is used to connect the flap torsion spring to the flap hinge.
$\boldsymbol{L_L}$	is the arm that is used to connect the lag torsion spring to the lag hinge.
$\boldsymbol{L_{S_F}}$	is the leg length for the torsion spring that is used for flap.
$\boldsymbol{L_{S_L}}$	is the leg length for the torsion spring that is used for lag.
$\boldsymbol{m}$	is the mass of the blade.
$\boldsymbol{m}$	is the total moving mass experienced by the VCM.
$\boldsymbol{m_{eff}}$	is the effective mass of the demonstrator experienced by the pitch actuator.
$\boldsymbol{M_F}$	is the moment around the flap axis.
$\boldsymbol{M_S}$	is the torsional moment of the torsion spring.
$\boldsymbol{P}$	is the power dissipation for the actuation of pitch.
$\boldsymbol{P_C}$	is the continuous power of the VCM.
$\boldsymbol{r}$	is the arm at which pitch is actuated.
$\boldsymbol{R}$	is the resistance of the VCM.
$\boldsymbol{t}$	is the time.
$\boldsymbol{t}$	is a design parameter of the flexure; it represents the leaf thickness.
$\boldsymbol{T}$	is the cycle time for the actuation of cyclic pitch.
$\boldsymbol{T(t)}$	is a function of time that is needed to describe the deflection of a bending beam.
$\boldsymbol{w}$	is a design parameter of the flexure; it represents the width of the mechanism.
$\boldsymbol{x}$	determines the position on a beam.
$\boldsymbol{x(t)}$	is the function that describes the positional output of the linear pitch actuator.
$\boldsymbol{\dot{x}_{max}}$	is the maximum velocity that is required for the actuation of pitch.
$\boldsymbol{\ddot{x}_{max}}$	is the maximum acceleration that is required for the actuation of pitch.

$\boldsymbol{X}$	is the total stroke for the pitch actuator.
$\boldsymbol{y}$	is the deflection of a bending beam.
$\boldsymbol{dy}$	is the deflection of the flexure at a certain load.
$\boldsymbol{Y(x)}$	is a function of displacement that is needed to describe the deflection of a bending beam.
$\boldsymbol{\beta}$	is a variable that is needed to calculate the natural bending frequency of a beam that has a rotational stiffness at one side.
$\boldsymbol{\theta}$	is the rigid body flapping angle of a blade.
$\boldsymbol{\theta}$	is the angle change of a hinge of the flexure at a certain load.
$\boldsymbol{d\theta}$	is the angle change of the torsion spring for the derivation of the required leg length.
$\boldsymbol{\Theta}$	is the angle amplitude for the actuation of pitch.
$\boldsymbol{\rho}$	is the mass density per unit length of a beam.
$\boldsymbol{\phi}$	is the angle of the blade for te derivation of the natural bending frequency.
$\boldsymbol{\varphi}$	is a characteristic of a cross hinge; it represents the angle of the leafs.
$\boldsymbol{d\varphi}$	is the angle change of the blade for the derivation of the required torsion spring leg length.
$\boldsymbol{\omega_n}$	is the natural bending frequency of a beam.
$\boldsymbol{\Omega}$	is the symbol for the operation frequency of both the RBS and the demonstrator.

Contents

1. Introduction

Rotor Blade Systems (RBS) such as helicopters and wind turbines are complex structures with complex behavior. Systems like these make use of flexible rotating blades that display several types of deformations while they are in operation. The rotor and blades are an important source of vibrations in RBS [1]. For the case of the helicopter, this is shown in figure 1.1. As can be seen in this figure, frequencies resulting from the main rotor are predominant throughout most of the fuselage. If the rotor or one of the blades of an RBS would be damaged, it would most likely result in unwanted vibrations in the rest of the system. For this reason, it would be favorable to monitor the behavior of the rotor and blades for maintenance purposes, so that rotor damage can be detected in an early stage and more targeted maintenance can be performed. This can lead to a decrease of downtime due to unplanned maintenance. Vibration monitoring of RBS is however not so advanced [2].

With the development of autonomous Wireless Sensor Networks (WSN) such as the WiBRATE Project, new possibilities regarding vibration monitoring arise. The WiBRATE Project deals with the development of wireless self-powered vibration sensors that make use of wireless communication [3]. With this technology in development, new possibilities regarding on-blade monitoring arise, which is considered to be a significant improvement [2]. To explore the possibilities of on-blade monitoring in RBS, it is useful to build a demonstrator that represents an RBS. For this master assignment, an experimental setup that represents a helicopter RBS was designed and built. This demonstrator can be used to test different strategies for on-blade monitoring in RBS.

This assignment was performed under the chair of Applied Mechanics at the University of Twente. This section is part of the Faculty of Engineering Technology. Rotor dynamics are an interesting subject for this chair. Parallel with the research described in this report, another study regarding RBS was performed by Stefan Oosterik [4], in which an analytical model of a helicopter rotor was developed. These two theses together will be used as a basis for further research of on-blade monitoring in RBS. This introducing chapter will go more into detail on RBS. Furthermore, the objectives of this thesis are described. The chapter ends with an overview of the outline of this report.

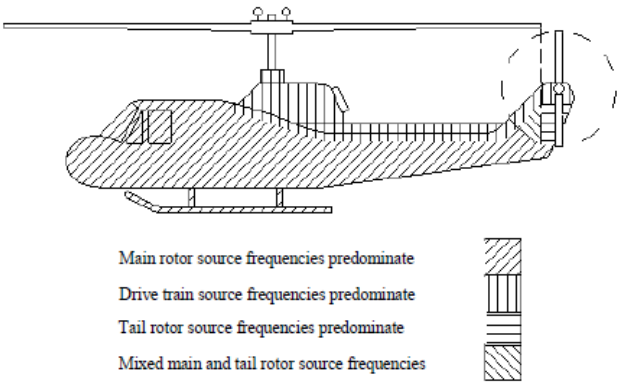

Figure 1.1: Helicopter vibration zones [1]

1.1 Rotor Blade Systems

This section will go more into detail on RBS. As mentioned, RBS make use of flexible rotating blades that display several types of deformations. These Degrees Of Freedom (DOFs) are described in this section. Next, the complexity of monitoring RBS is explained, followed by a comparison between helicopters and wind turbines.

1.1.1 Degrees Of Freedom in RBS

Figure 1.2 shows the different DOFs of an RBS. The DOFs shown in figure 1.2a are feathering, flapping and lead/lagging. Figure 1.2b shows the axes for the rigid and elastic body DOFs. The different DOFs will now be described. The first degree of freedom that is described is pitch, which is the rigid feathering mode of the blade. Pitch is the only DOF that can really be controlled from outside. The rest of the DOFs depend on other factors, such as flight or weather conditions, aerodynamics and blade loading.

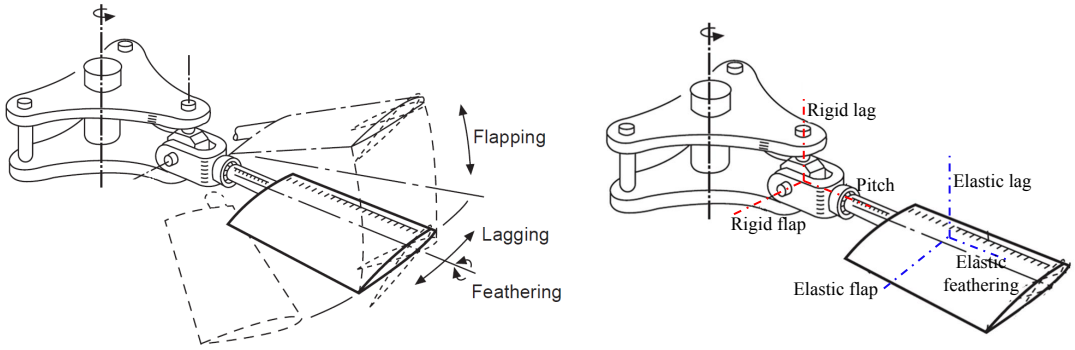

(a) DOFs of an RBS

(b) Rigid and elastic DOFs

Figure 1.2: Degrees of freedom of an RBS rotor [5]

Pitch

As mentioned, pitch is the only DOF that is fully controlled. Pitch is the rigid twist of the blade around the radial axis. Figure 1.3 represents the cross section of an RBS blade. In this figure, θ represents the pitch angle. Two types of pitch exist; collective and cyclic pitch. A change in collective pitch changes the pitch angle of all the blades with the same amount, while a change in cyclic pitch changes the pitch angle over each rotation.

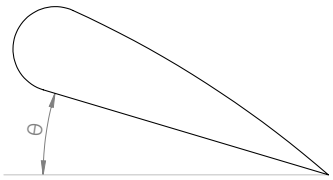

Figure 1.3: Blade pitch angle

In wind turbines, cyclic pitch is usually not present. The collective pitch angle determines the amount of torque that the wind generates on the rotor; when the pitch angle is changed, the angular velocity of the rotor will change if the other conditions stay the same.

In a helicopter, pitch is used to control the position of the helicopter. Pitch is usually controlled by two swashplates. Swashplates exist of two plates, one is rotating, while the other is non-rotating. The plates

are used to control both cyclic and collective pitch. The principle of swashplates and is explained in the figure 1.4. Figure 1.4a shows the side view of a helicopter rotor with the vertical axis of rotation and two blades at opposite sides of the rotor. The swashplates consists of two plates: the blue plate is connected to the blades and is rotating, while the red one is not rotating. The red plate is actuated to control its height and angle. In figure 1.4b, the height of the red plate is increased. As can be seen, this changes the collective pitch angle; the pitch angle of the two blades in the figure changes with the same amount. The amount of lift that the rotor generates is controlled by collective pitch. Figure 1.4c shows a change in the angle of the red plate. As can be seen, the change of the pitch angle differs for the two blades in the figure. When cyclic pitch is changed, the pitch angle of each blade changes individually. A change in cyclic pitch results in a change of lift distribution over the rotor disk area. The horizontal movement of a helicopter is controlled with cyclic pitch.

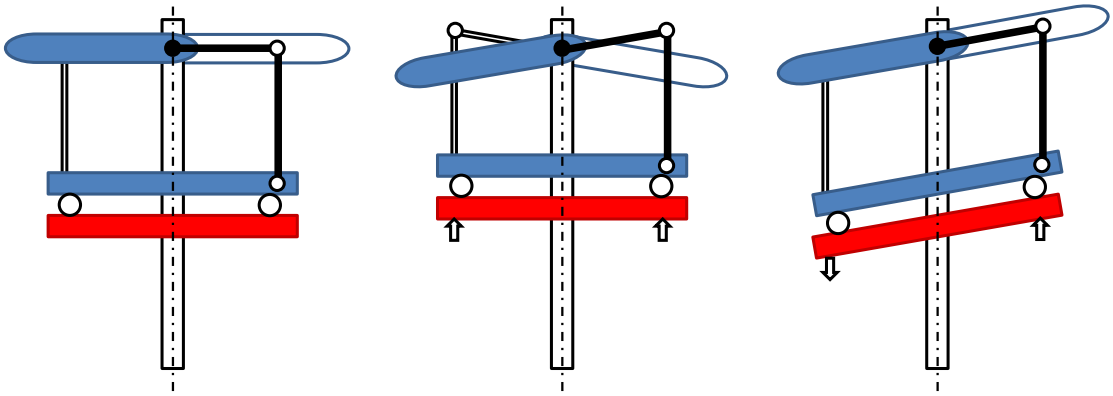

(a) Swashplate (b) Collective pitch (c) Cyclic pitch

Figure 1.4: Cyclic and collective pitch in swashplates

Feathering

Feathering is the twist of the blade around the radial axis. Two types of feathering can occur in operation; rigid and elastic feathering. Rigid feathering changes the pitch angle of the total blade. As described, this type of feathering is controlled. Besides rigid feathering, elastic feathering occurs due to the aerodynamic loads on the blade [6]. Unlike rigid feathering, elastic feathering is not controlled. Because of elastic feathering, the blade pitch angle changes over the length of the blade. Therefore, this type of feathering is unwanted and the torsional stiffness of the blade is usually high [7].

Flapping

Flapping is the up and down movement of the blade. It occurs in response to the changes in lift or velocity due to cyclic pitch [8]. Flapping is a harmless movement of the blade. In fact, it is wanted in helicopters to compensate dissymmetry of lift that occurs in case of horizontal flight.

Lead-lag

Lead-lagging (lagging) is the forward and backward movement of the blade in the plane of rotation. When a blade is flapping, it experiences Coriolis moments in the plane of rotation. These moments cause the lagging motions [5].

Overview of DOFs

The DOFs described in this section are all DOFs of the RBS. To get a better overview, the characteristics of the DOFs are presented in table 1.1. A schematic picture of the helicopter RBS and its DOFs is drawn in figure 1.5.

Table 1.1: Characteristics of the different DOFs in RBS

DOF	Type	Wanted?	Controlled?
Pitch	Rotor	Wanted	Controlled
Rigid flap	Rotor+blade	Wanted	Not controlled
Rigid lag	Rotor+blade	Unwanted	Restricted by rotor damping
Elastic flap	Blade	Wanted	Not controlled
Elastic lag	Blade	Unwanted	Not controlled
Elastic torsion	Blade	Unwanted	Not controlled

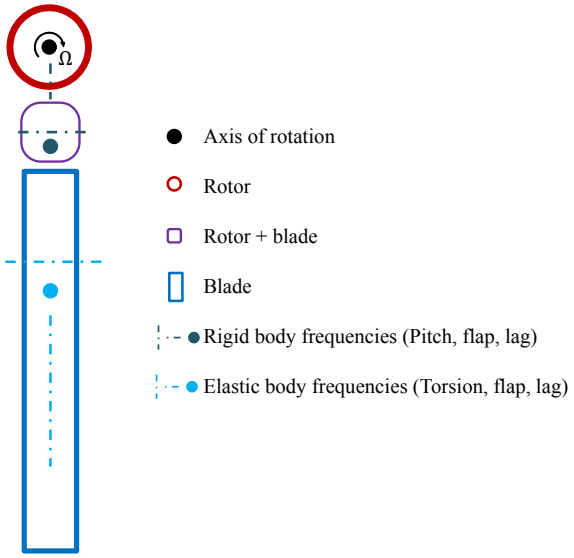

Figure 1.5: Degrees of freedom of the RBS

1.1.2 Complexity

Due to the rotation, the blades of an RBS experience different effects; centrifugal effects result in an added rotational stiffness and radial loading, while a change in rotational inertia caused by relative motions of the blade can lead to Coriolis and gyroscopic effects that result in coupling of motions. Furthermore, the aerodynamic loading on the blades is highly dependent on the flight (helicopters) and weather (wind turbines) conditions. These are all effects that make monitoring of RBS complex [4].

1.1.3 Helicopters and wind turbines

Wind turbines and helicopters are both RBS. These systems share many similarities; they both make use of flexible rotating blades to fulfill their function. Besides, the systems display similar DOFs. However, some differences have to be pointed out. The most important differences between helicopters and wind turbines are listed in table 1.2. This table states that the blades of the helicopter do not experience fatigue loading due to gravity. It should however be mentioned that this does not mean that the blades of a helicopter do not suffer from fatigue.

Table 1.2: Differences between helicopter and wind turbine rotors

	Helicopter	**Wind turbine**
Function	Generate lift	Generate power
Driving force	Motor power	Wind
Location of power	On the rotor	On the blades
Rotor frequency	Constant (±4Hz) [5]	Depends on wind and pitch
Pitch	Both cyclic and collective	Collective
Internal moments	Depending on type of rotor (Sec. 2.1.3), some moments can be released through hinges	Hub has to deal with moments
Gravity	Direction of axis of rotation; blades experience constant gravitational loads, gravity does not contribute to fatigue problems	Perpendicular to axis of rotation; gravity contributes to fatigue when the system is in operation

As mentioned, this thesis was performed parallel with a thesis in which an analytical model of a helicopter rotor was developed [4]. These theses together will be used as a basis for further research on how on-blade monitoring can be of value in RBS, e.g. to investigate the detectability of certain damage scenarios. To be able to combine these studies more easily, the focus of this thesis will be on helicopter RBS.

1.2 Assignment objective

As stated in the introduction of this chapter, it is useful to build a demonstrator that represents an RBS to explore the possibilities of on-blade monitoring in RBS. This thesis focuses on the design and construction of such a demonstrator that represents the behavior of an RBS. The following objectives are defined:

- Investigate the added value of on-blade monitoring in RBS by generating an overview of previously performed experiments regarding RBS.
- Design and build a functional setup that represents the behavior of an RBS. This demonstrator is expected to display the different DOFs; flap, lag and feathering.

The first objective aims at generating more insight in the research that has been done regarding RBS and conclude if and how the different experiments could have benefited if on-blade monitoring was an option. Furthermore, investigation of the different experimental setups might help during the design process of the demonstrator.

Due to the complexity of an RBS, it is not realistic to build a demonstrator that fully represents its behavior. Therefore, the complexity will be reduced for the demonstrator, while the behavior will still be represented.

1.3 Thesis outline

This chapter introduces the problem and the objectives of this thesis. The last section of this chapter contains an outline of this thesis report.

- **Chapter 2** contains the literature review that was performed for this research. The RBS is described into more detail. Furthermore, previous performed experiments regarding RBS were reviewed. The results and conclusions of this review are given in this chapter.

- **Chapter 3** describes the first phase of the design process. On the basis of a Function-Behavior-Structure framework, the design requirements for the demonstrator are listed. The chapter describes how the complexity of a helicopter RBS is reduced and how its behavior will be represented by the demonstrator. Besides, the procedure that is followed to come up with the design of the demonstrator is described and the first decisions that were taken during are listed and motivated.
- **Chapter 4** presents the design of the demonstrator. The end result is first presented, followed by the design of the different subsystems.
- **Chapter 5** describes the design of the surrounding subsystems of the demonstrator, i.e. the actuation and the frame.
- **Chapter 6** describes the experiments that were performed with the demonstrator.
- **Chapter 7** contains the conclusions of this thesis. Furthermore, recommendations for further research are given.

2. Literature

To be able to come up with a design for the demonstrator that represents a helicopter RBS, it is important to gather the required information about systems like these. For this reason, the literature was reviewed to generate the required knowledge. Besides collecting the necessary information on helicopter systems, the literature was reviewed for another reason, i.e. to review the experimental research that was performed regarding (rotating) blade systems. This chapter will describe this literature review.

2.1 RBS

This section will describe the helicopter RBS into more detail. This will be done in the Function-Behavior-Structure (FBS) framework. The FBS framework is often used to describe the different aspects of a design object. Three types of variables form the basis of the FBS framework [9]:

- **Function variables**: These describe the purpose of the object, i.e. what it is for.
- **Behavior variables**: These describe the characteristics that can be derived from the object's structure, i.e. what it does.
- **Structure variables**: These describe the components of the object and their relationships, i.e. what it is.

The FBS framework is often used as a guideline for design processes. In this case, it will be used the other way around, i.e. to describe a system that already exists; the helicopter RBS.

2.1.1 Function

The first variable of the helicopter rotor, the function, is to generate and control the amount of lift to be able to control the position and speed of the helicopter. This lift is generated by the rotation of the blades. Both the horizontal and the vertical position and speed are controlled by the rotor; vertical movement is controlled by the collective pitch, while the horizontal movement is controlled by adjusting the cyclic pitch.

2.1.2 Behavior

In section 1.1.1, the DOFs present in RBS are described. These motions are part of the behavior of the RBS. However, it is not clear yet how these DOFs are related to each other in an RBS.

To get an overview of the different modes that are present in a RBS, the natural frequencies of a rotating blade should be clear. For his PhD thesis, Pieter de Jong determined the natural frequencies of a fully articulated helicopter rotor (Sec. 2.1.3) with a blade of length $R = 8.15$m in ANSYS [10]. The first eight modes that were determined in this analysis are shown in table 2.1. The frequencies in this table are in terms of the rotor frequency Ω. The two bold modes in this table, i.e. the first flapping and lagging

mode, are the rigid body modes of the system. The rest of the modes are elastic modes, they represent the natural frequencies of the blade.

Table 2.1: First blade natural frequencies in terms of rotor frequency Ω [10]

Mode	Ω
Lag 1	**0.3**
Flap 1	**1.04**
Flap 2	2.68
Lag 2	4.56
Flap 3	5.35
Feathering 1	5.82
Flap 4	9.65
Lag 3	11.9

Damage scenario

Consider the helicopter rotor that was used for the determination of the mode frequencies of table 2.1. Now suppose that this rotor has one damaged blade, it is likely that the mode frequencies presented in table 2.1 shift for this specific blade. If for example a crack develops in the blade at the red dashed line in figure 2.1, the consequence will be that the flapwise stiffness of the blade decreases. Therefore it is likely that the mode frequencies for flapping will decrease as well, while the frequencies corresponding with the other modes are not likely to change that much.

When on-blade monitoring would be used on a helicopter, knowledge of the mode frequencies of the undamaged system can be useful. If the measured mode frequencies turn out to differ with respect to the 'normal' values, it might be because of a starting damage in the system. By detecting this starting damage in an early stage, the maintenance that is required can be targeted and the unplanned downtime of the helicopter can be reduced.

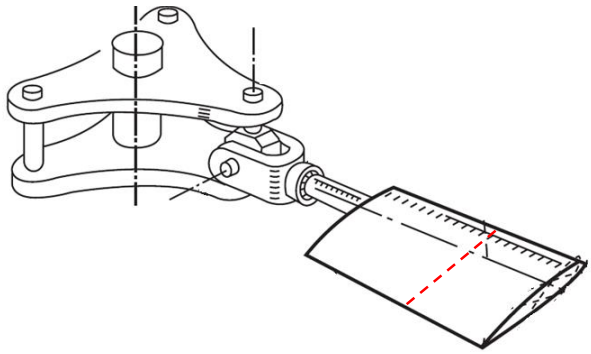

Figure 2.1: A damage scenario for the helicopter blade

2.1.3 Structure

A helicopter RBS can be divided into three components, i.e. the actuation, the hub and the blade. The function of actuation is to generate the rotating movement. The hub is the connecting component, the most important function of the rotor hub is to restrain unwanted DOFs and to deal with the high moments and forces. The blade is the component that generates the lifting force. Besides generating lift, the blade has to deal with the internal DOFs.

Although every helicopter RBS consists of these components, different types of helicopter rotors exist,

for which the structure and the properties differ. Three different main types of helicopter rotors can be pointed out:

- Rigid or hingeless rotor
- Semi-rigid rotor
- Fully articulated rotor

The characteristics of these rotor types will now be described according to the Helicopter Flying Handbook [8]. In each of the figures presented, the black dashed line represents the axis of rotation of the rotor, a yellow line represents a pitch axis, a red line represents the axis of a flap hinge and a blue line represents the axis of a lag hinge.

Rigid rotor

The rigid or hingeless rotor is mechanically the most simple type of the three rotor types described. The blade roots are rigidly attached to the rotor hub, so the loads due to the different modes are absorbed by the hub. For flap and lag, the rigid body modes will not be present in the rigid rotor, because of the rigid attachment. In other words, this rotor can only display elastic modes for flap and lag. The only rigid blade mode available in this rotor is the pitch. To compensate for dissymmetry of lift, the blades should be flexible enough to be able to flap while the helicopter is in operation. An example of a rigid helicopter rotor is shown in figure 2.2.

Semi-rigid rotor

The semi-rigid rotor system usually consists of two blades which are rigidly connected to the rotor hub. This hub can tilt with respect to the rotor shaft, so the blades can flap together as a unit. As for the rigid rotor system, the loads due to the lagging modes will be absorbed by the hub. However, because of the tilting of the hub, no moments due to flapping will be transferred to the rotor hub. A semi-rigid helicopter rotor is shown in figure 2.3.

Fully articulated rotor

The fully articulated rotor system is mechanically the most complex one of the three. In this type of rotor, the blades can flap and lag independent of the other blades. Due to the presence of flap and lag hinges, no moments due to flap and lag are transferred to the rotor hub. Figure 2.4 shows a fully articulated helicopter rotor.

2.2 Previous experiments

A literature review of previous experiments regarding blade systems was performed. The goal of this review was to get an overview of the possibilities on monitoring RBS. For this review, not only experiments that covered research on helicopters were reviewed, different types of experiments were reviewed. From old experiments like Ormiston's in 1972 [14] or Caradonna's in 1981 [15] to more recent studies like a series of wind tunnel experiments part of the GOAHEAD project performed between 2005 and 2009 [16], from complex experiments with complete assembled rotors like NASA's [17] to less complex experimental setups like Ozcelik's that only contained a flapping beam [18]. Table 2.2 gives a compact overview of the different reviewed experiments. The second column of this table indicates the system for which this research was performed; helicopters, wind turbines or beams. Some of the experiments will be discussed into more detail in this section.

Figure 2.2: Rigid rotor [11]

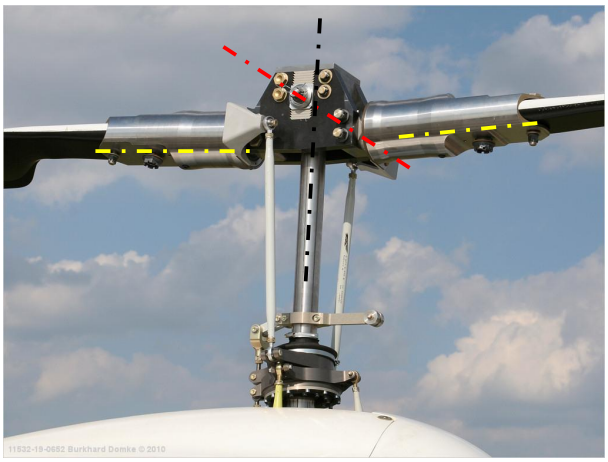

Figure 2.3: Semi-rigid rotor [12]

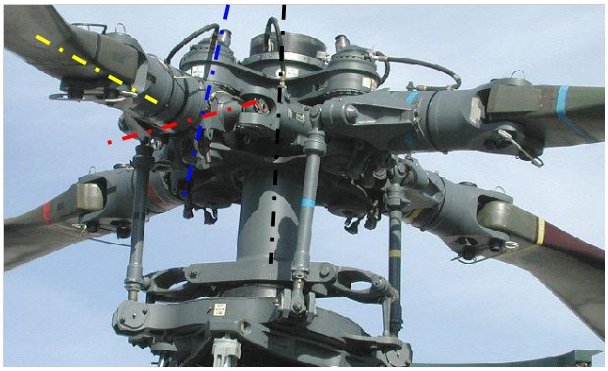

Figure 2.4: Fully articulated rotor [13]

Table 2.2: Reviewed previous experiments

Experiment	**Type**	**Experiment properties**
Büter [19]	H	Non-rotating experiments Goal: Improve helicopter characteristics with adaptive blade twist
Özbek [20]	WT	Optical measurements on wind turbines Field measurements on wind turbines in operation Goal: Get more insight in the dynamic properties of large wind turbine blades
GOAHEAD [16, 21, 22]	H	Series of subscale helicopter wind tunnel experiments Goal: Create a deeply analyzed experimental database
Ozcelik [18]	B	Non-rotating experiment with a flapping beam Goal: Examining non-linear structural dynamics of a flapping beam
Ormiston [14]	H	Both rotating and non-rotating experiments with a hingeless helicopter rotor Goal: Validate theoretical analysis and gather more information on hingeless rotor blades
Caradonna [15]	H	Rotating experiments for helicopter rotors in hover Goal: Aid the development of various rotor performance codes
Monteiro [23]	WT	Rotating wind tunnel experiments for scaled wind turbines Goal: Validate Blade Element Momentum codes
NASA '80s [24]	H	Both rotating and non-rotating tests with a small scale hingeless helicopter rotor Goal non-rotating experiments: Determine non-rotating modal frequencies and lead-lag structural damping Goal rotating experiments: Determine lead-lag stability characteristics and steady state bending moments
NASA '90s [17]	H	Full scale rotating helicopter rotor tests Goal: Get rotating blade frequencies and compare results with analytical predictions
Riemenschneider [25]	H	Rotating experiments with on-blade measurements Goal: Deliver reliable data of blade twist actuation in the rotating system
Bin Yang [26]	WT	Series of wind turbine tests Static tests, fatigue tests, modal analysis and full scale testing Goal: Test, inspect and monitor blades to guarantee service safety
Malhotra [27]	WT	Non-rotating tests with large wind turbine blades Static testing and fatigue testing Goal: Development and design of a dual-axis blade testing method for larger wind turbine blades to control if they fulfill their specifications

Abbreviations

H	Helicopter
WT	Wind turbine
B	Beam

2.2.1 On-blade monitoring in the rotating system

Four of the reviewed experiments made use of on-blade monitoring in the rotating system, i.e. the two experiments of NASA [17, 24], the GOAHEAD project [16, 21, 22] and Riemenschneider's research [25]. These experiments will first be described.

NASA '80s

The experiments described in the technical report of Sharpe were performed for NASA in the 1980s [24]. The goal of this research was to generate more knowledge about the characteristics of hingeless helicopter rotors; these rotors were relatively new in the time of this research. Non-rotating tests were performed to determine the modal frequencies and lead-lag structural damping. For the non-rotating tests, all DOFs were being monitored.

Besides these tests, rotating tests were performed to determine stability characteristics for lagging motion. Only lagging was monitored for the rotating tests. The rotating frequencies could only be calculated, no attempts were made to determine these experimentally, since this was not possible with the available equipment. For both types of tests, lagging was the only excited DOF, this was done by a shaker.

NASA '90s

In the 1990s, another research regarding helicopters was performed by NASA, which is described in the technical report of Keats Wilkie [17]. The tests performed for this research made use of a four-bladed fully articulated rotor hub. The experiment described in the report was performed to evaluate a modified finite element method, which includes rotational effects for hub designs. The tests were conducted in the Langley Helicopter Hover Facility, a high-bay facility for hover testing, see figure 2.5.

Figure 2.5: Helicopter Hover Facility for NASA's experiments

This experiment made use of on-blade monitoring, but instrumentation of the blade was limited. For this reason, only elastic blade frequencies up to and including the first elastic feathering mode were measured. Besides, no attempt to measure the blade mode shapes was made.

The rotating blade frequencies that were measured were compared to the analytical values predicted with the finite element method. The flapping and lagging modal characteristics were adequately predicted with slight modifications, while accurate predictions of the torsional frequencies require some extra modifications in the code.

GOAHEAD

For the GOAHEAD (Generation Of an Advanced Helicopter Experimental Aerodynamic Database) project, multiple wind tunnel experiments were performed with a scaled model of a complete helicopter. Main goal of this project was to create an experimental database for the validation of 3D computational fluid dynamics and comprehensive aeromechanics methods for complete helicopter configurations [16,22]. For these wind tunnel experiments, more than 800 sensors were used for all the measurements. Most of these sensors were located on the helicopter fuselage, however, strain gages and pressure transducers were also used on the rotor and blades. The GOAHEAD project succeeded in creating a comprehensive database with data and documentation for complete helicopters. Besides, the CFD solvers that were applied were capable to perform simulations with good accuracy.

Riemenschneider

The experiment of Riemenschneider [25] also made use of on-blade monitoring in the rotating system. Multiple strain gages were used to retrieve data of the blade. Instrumentation of this experiment was described to be a complex procedure, due to the many wires running through the blade. The setup of this experiment consisted of a single rotating blade, of which the pitch was controlled. The research focused on the design and evaluation of a reliable measuring concept that would be used to generate data about the blade actuation. The most complex part of this was to determine the blade tip twist angle. It was concluded that it was impossible to determine this angle with acceleration sensors, so optical measurements were performed to determine it.

2.2.2 Other type of experiments

The experiments just described all made use of on-blade monitoring in the rotating system. Besides these, other experiments that did not make use of on-blade monitoring in the rotating system were reviewed. Some of these experiments will now be described.

Ormiston

As for NASA's tests in the 1980s, the experiment described by Ormiston aimed at gathering more knowledge about hingeless helicopter rotors [14]. Both rotating and non-rotating tests were performed. The goal of these non-rotating tests was to measure the bending moments of the blades which are caused by flap and lag. The rotating tests examined both steady state and transient operation. For the transient tests, a shaker was used to excite the fixed hub in a direction parallel to the plane of rotation. This excitation was done at the lagging natural frequency.

The research has provided more knowledge about the behavior of hingeless helicopter rotors. In the time of this research (1972), hingeless helicopter rotors were not widely used, so for a rational approach to the design of these systems, more knowledge about the behavior of these rotors was important.

Adaptive blade twist

The experiment described in the paper of Büter [19] investigates adaptive blade twist for helicopters. With this concept, the twist (feathering) of the blades could directly be controlled by smart adaptive elements. Goal of this technology was to improve the helicopter's characteristics; e.g. reduce noise. For the experimental investigations of this research, feathering was controlled. Besides, three eigen modes were excited separately; two flap modes and one feathering mode.

Wind turbine blade testing

As the size of wind turbines becomes bigger, the necessity of testing, inspecting and monitoring the blades increases to be able to guarantee their service safety. The paper of Bin Yang [26] describes different technologies to test these wind turbine blades, of which the fatigue tests are interesting for this research. These fatigue tests were performed for both flap and lag, but these tests were performed separately from each other. The paper of Malhotra [27] also deals with the testing of large wind turbine blades. This research introduces a new type of testing, in which flap and lag are excited simultaneously for the fatigue tests. This method of excitation might be interesting to consider when both flap and lag are to be excited for the demonstrator.

Monitoring of wind turbines

For Özbek's PhD thesis [20], optical measurements on wind turbines in operation were performed. This was done with the goal to generate more knowledge about the dynamic properties of large wind turbines. The setup of these measurements is shown in figure 2.6. The wind turbine was monitored from three different positions at large distance from the turbine. Multiple markers were installed on the blades to be able to monitor the system more accurately. The accuracy of these measurements will depend on several factors, both controllable (e.g. camera resolution) and uncontrollable (e.g. the weather). Due to the large distance between the cameras and the wind turbine, the accuracy of the data can be questioned.

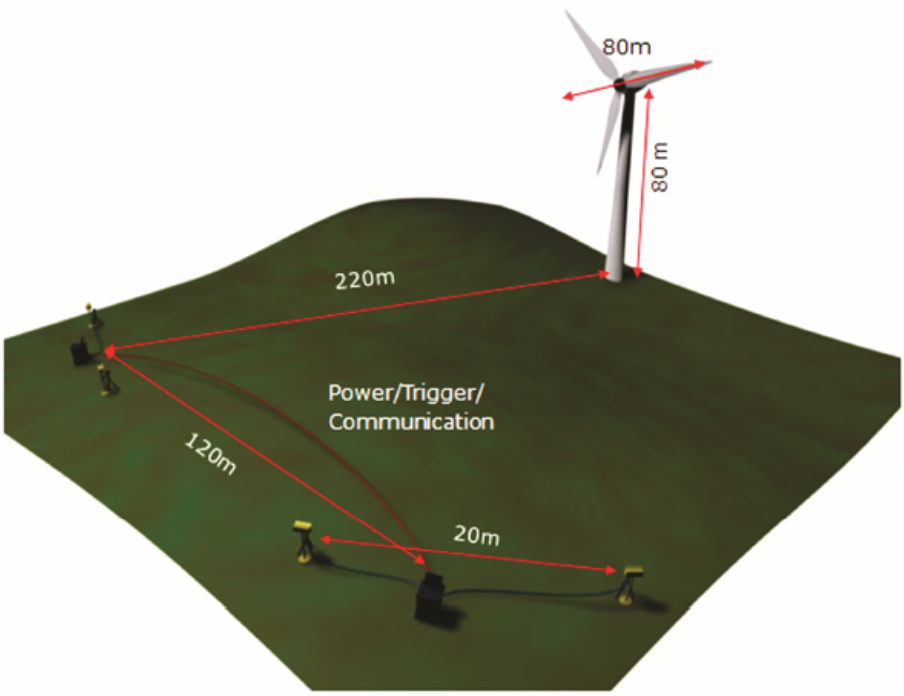

Figure 2.6: The measurement setup of Özbek's research [20]

2.3 Classification of experiments

Table 2.2 of the previous section lists the experiments that were reviewed. This table does not give a clear image of the setups of these experiments yet. Besides, the purpose of the research differed between the reviewed experiments. To get a better overview of the different reviewed experiments, they were classified on the basis of purpose and experimental setup.

The classification on the basis of the main purpose is shown in table 2.3. For the demonstrator of this thesis, the goal is to test monitoring strategies for maintenance purposes, so it would be classified best in the last column of the table.

Table 2.3: Main goals of the reviewed experiments

Performance/control	**Validation of software codes**	**Generate insight in the behavior**	**Service/maintenance testing**
Büter Caradonna Riemenschneider	GOAHEAD Ormiston Monteiro NASA 90s	Ozcelik Özbek NASA 80s	Bin Yang Malhotra

The classification of the setups of the different experiments is done on the basis of the DOFs which were being excited and monitored. This classification is shown in table 2.4. As can be seen, the table is divided into four quarters. This division is made on the basis of the number of DOFs that are monitored and excited. The experiments in the first quarter excite and monitor maximum one DOF, while for the experiments of the fourth section the number of excited and monitored DOFs are both at least two.

Table 2.4: Classification of the reviewed experiments

		MONITORED DOFS							
		None	**Fe**	**Fl**	**L**	**Fe+Fl**	**Fe+L**	**Fl+L**	**Fe+Fl+L**
EXCITED DOFS	**None**	[15](R) [23](R)						[20](R)	[16](R)
	Fe					[25](R)			[17](R)
	Fl	[26](NR)		[18](NR)					
	L	[26](NR)			[24](R)			[14](R)	[24](NR)
	Fe+Fl		[19](NR)						
	Fe+L								
	Fl+L	[27](NR)						[14](NR)	
	Fe+Fl+L								

References

[14] Ormiston
[15] Caradonna
[16] GOAHEAD
[17] NASA '90s
[18] Ozcelik
[19] Büter
[20] Özbek
[23] Monteiro
[24] NASA '80s
[25] Riemenschneider
[26] Bin Yang
[27] Malhotra

Abbreviations

Fe Feathering
Fl Flap
L Lag
R Rotating
NR Non-rotating

2.4 Conclusion of experiments

Many of the reviewed experiments could be improved with on-blade monitoring. When looking at table 2.3, the experiments in the last two columns seem most likely to benefit when on-blade monitoring is fully available. For example, the accuracy of the measurements performed in the research of Özbek could be significantly improved when the wind turbine blades were directly monitored by making use of on-blade

sensors. By doing this, the accuracy of the measurements does not depend on uncontrollable factors such as the weather anymore. For the tests in the last column, the fatigue tests of wind turbine blades performed in the experiments of Bin Yang and Malhotra, developing fatigue cracks could be detected in an earlier stage with on-blade monitoring.

As can be concluded from the classification of the reviewed experiments, not much experimental research has been done where multiple DOFs are excited and monitored, i.e. the shaded quarter in table 2.4. When on-blade monitoring will be implied in RBS it is favorable that all DOFs are being monitored, to be able to detect different damage scenarios.

Taking in mind the demonstrator that is to be built and the possibility to monitor multiple DOFs with on-blade monitoring, it would be favorable for the demonstrator to have at least two DOFs actively excited. By doing this, the demonstrator can be classified in the not widely explored shaded quarter of table 2.4.

3. Design process

The first chapters of this report described the problem and provided required knowledge on the subject of this thesis. This chapter will go into detail on the first phase of the design process. The demonstrator will first be described through the FBS framework. After this, a set of design requirements for the demonstrator is listed. On the basis of the FBS-framework and the design requirements, the design procedure that is followed is described. Furthermore, the first design decisions that were taken are described and motivated at the end of this chapter.

3.1 Function

With the FBS of the helicopter rotor described in the previous chapter, the characteristics of the demonstrator that are desired become more clear. This FBS framework was done to get a better understanding of the RBS. The FBS framework will also be used as a guideline for the design of the demonstrator.

The function of the demonstrator is to represent the behavior of a helicopter RBS. As stated in section 1.2, the complexity will be reduced for the demonstrator, so the desired behavior should be clear. The list below sums up the different types of behavior of a helicopter RBS.

- Rotation of blades
- DOFs (Flap, lag, feathering)
- Vary pitch angle to control the position of the helicopter
- Display modes according to table 2.1

3.2 Behavior

The decision of what kind of behavior is desired for the demonstrator is an important one, because the design fully depends on it. For rotating scaled rotor models, the blade tip speed is considered to be an important parameter to keep constant [28]. If for example a 50% scaled rotor model will be used, the rotational velocity will have to be doubled to keep the blade tip speed constant. In other words, the rotational velocity will change in inversely proportion with the scaling. Taking in mind the available space for the demonstrator, scaling will certainly be necessary for the demonstrator. Due to the safety precautions that have to be taken with the resulting high rotational velocity of the system, the rotating aspect is the first type of behavior that was excluded.

The desired behavior of the demonstrator is listed as follows:

- Display flap, lag and rigid feathering
- Control cyclic pitch

- Display the first three modes according to table 2.1

This means that the demonstrator should be able to display all DOFs. As explained in section 1.1.1, cyclic pitch is the change of pitch over each rotation. This can be simulated in a non-rotating system by actuating the pitch angle with a sinusoidal function. The frequency of this function will represent the rotor frequency Ω. The third type of desired behavior listed regards table 2.1. The frequencies of the first three modes, i.e. rigid lag (f_{l_r}), rigid flap (f_{f_r}) and the first elastic flapping mode ($f_{f_{el,1}}$) should be in the same range with respect to the actuation frequency Ω as in the table. This means that one frequency can be chosen out of Ω, f_{f_r}, f_{l_r} and $f_{f_{el,1}}$, while the other three are then decided.

3.3 Structure

This section describes the structure of the demonstrator to complete the FBS-framework. It will first describe the rotor type that should be represented. Next, the actuation of the system will be discussed. Furthermore, the structure of the demonstrator will be described as a series of subsystems.

Rotor type

With the desire to let the demonstrator display the first couple of modes according to table 2.1, the rotor type that should be represented by the demonstrator is already clear. To be able to display both rigid flap and lag, the demonstrator should contain hinges for these DOFs, which means that it represents a fully articulated rotor.

Actuation

For the actuation, it should be decided which modes will be actuated. In a helicopter, rotation and pitch are directly actuated by the engine and the pilot, while flap, lag and elastic feathering are a result of the rotation of the blades, aerodynamic loads, Coriolis forces and unequal lift distribution over the rotor disk.

For the demonstrator, the actuation of pitch should be at constant frequency Ω, because this is also the case in helicopters. For the other modes, actuation at constant frequency will not give a realistic image of the situation in helicopters. If these other modes will be actuated, this should be done at a broadband frequency signal. A possible way to do this, is by actuating it with a noise signal from a shaker.

Subsystems

The total system of the demonstrator can be divided into several subsystems. As mentioned, the demonstrator should contain hinges for all these DOFs. Five different main subsystems can be pointed out, i.e. the blade, the three hinges and the actuation.

The sequence in which the hinges are ordered is important for the design, because the frequencies of the different modes depend on them. If for example the hinges for lag and pitch are located between the flap hinge and the blade, then these hinges experience the flapping movement that is released by the flap hinge. This means that the lag and pitch hinges should be considered in the design process of the flap hinge to realize the desired frequencies.

The design of the flap hinge determines two frequencies (f_{f_r} and $f_{f_{el,1}}$), while the lag hinge only determines one (f_{l_r}) and the pitch hinge none. To reduce the complexity of the design process, it is decided to have no other hinges located between the flap hinge and the blade. By doing this, the design of the other hinges will have no effect on the flapping frequencies. With the flap hinge directly connected to the blade, the lag hinge and pitch link remain. For the design of these hinges, the flap hinge should be

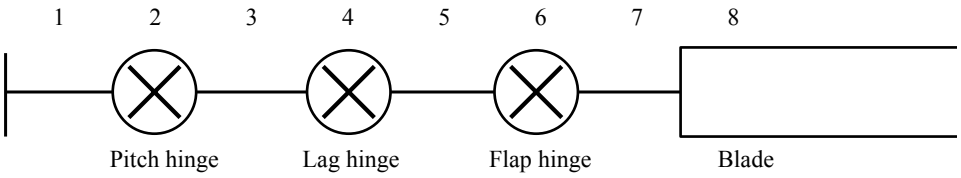

Figure 3.1: Global structure of the demonstrator

taken into account. Since the lag hinge determines one frequency and the pitch link determines none, it is decided to locate the lag hinge directly after the flap hinge, so that the design of the pitch link does not display lag and therefore does not affect the lagging frequencies. Besides, the fact that the pitch hinge does not display flap and lag makes it easier to actuate it. The global structure of the demonstrator without actuation is shown in figure 3.1. As can be seen, this figure shows eight subsystems, i.e. the four remaining main subsystems (blade and hinges) and the connections between them:

1. Connection between rigid world and the demonstrator
2. Pitch hinge
3. Pitch-lag connection
4. Lag hinge
5. Lag-flap connection
6. Flap hinge
7. Flap-blade connection
8. Blade

3.4 Design requirements

On the basis of the FBS analysis performed in the previous sections, a set of design requirements can be listed for the demonstrator. This section gives an overview of the design requirements. The requirements are classified into three different types; behavior, structure and monitoring requirements.

Behavior

- **DOFs:** The demonstrator should display flap, lag and rigid feathering.
- **Frequencies:** The frequencies Ω, f_{l_r}, f_{f_r} and $f_{f_{el,1}}$ should be related to each other as in table 2.1.

Structure

- **Rotor type:** The demonstrator should represent a fully articulated rotor; it must contain hinges for flap and lag.
- **Balancing:** The demonstrator should be self-balancing; there must be a neutral position to which it returns when displaying flap or lag.
- **Blade profile:** To be able to test different blade profiles, the demonstrator will have to be designed such that the blade can be easily replaced.
- **Pitch:** Pitch must be actuated at an operation frequency Ω that is to be chosen.

Monitoring

- **Operation frequency:** To keep the option of implementing a shaker open, the operation frequency (Ω) should be at least 10Hz. Many shakers have a frequency range that starts at 10Hz, so when a lower operation frequency is chosen, the usefulness of the low-frequent data can be questioned when a shaker is used.

- **DOFs:** Flap and lag should be monitored to be able to determine the different mode frequencies for which the demonstrator is designed.

3.5 Design procedure

Section 3.3 divided the total system of the demonstrator into five main subsystems. Several relations that are important to keep in mind during the design process exist between the different subsystems. The design procedure that was followed is schematically shown in figure 3.2. In this figure, black arrows define the path of the design process. The red dashed lines represent direct relations between the two elements it connects. K_{flap} and K_{lag} represent added stiffnesses in the hinges that are required to realize the desired frequencies for the corresponding modes.

The first thing that was done during the design process, was to choose the operation frequency Ω. With this frequency chosen, the resulting target frequencies f_{f_r}, f_{l_r} and $f_{f_{el,1}}$ are calculated to realize the same ratios as in table 2.1. After choosing Ω, the black box at the top of figure 3.2 is completely decided. With the desired frequencies known, the demonstrator was designed from section 8 to 1 according to the numbering of figure 3.1.

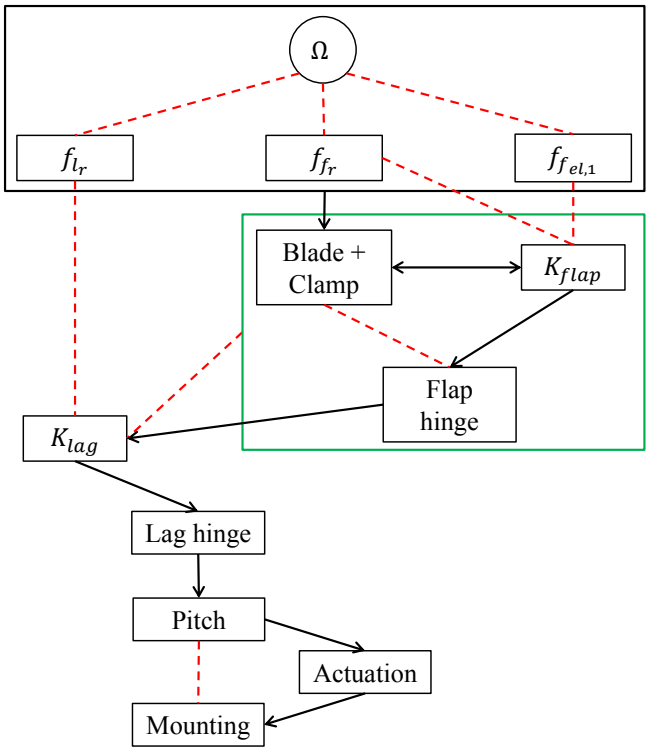

Figure 3.2: Design procedure for the demonstrator

3.6 First design decisions

This section gives an overview of the first decisions that were taken during the design process.

Operation frequency

As mentioned in the previous section, the operation frequency was the first thing that was chosen. The design requirements state that an operation frequency of at least 10Hz is required to gather useful data. Since an increase in the desired mode frequency will lead to an increase in the system's stiffness to be able to realize this frequency, it is decided to work with the minimal operation frequency ($\Omega = 10$Hz), to prevent the system from becoming too stiff. With this operation frequency, the desired frequencies for the three other modes are calculated:

- $f_{l_r} = 0.3\Omega = 3$Hz
- $f_{f_r} = 1.04\Omega = 10.4$Hz
- $f_{f_{el,1}} = 2.68\Omega = 26.8$Hz

Actuation

Besides actuating pitch at constant frequency Ω, it is decided to actuate flap as well. It is considered to be too complex to actuate both flap and lag besides pitch. Because the demonstrator has two desired frequencies for flapping modes while only having one for lag, excitation of flap is more interesting than it is for lag. Lagging can be activated by introducing an unbalance in lag, it will however not constantly be actuated.

Material

The main material used in the demonstrator is aluminium. The advantage of aluminium is that it has sufficient strength, without becoming too heavy.

Blade orientation

The demonstrator is required to be self-balancing. As mentioned in the FBS-framework, the demonstrator is not desired to display rotation. To realize the self-balancing requirement, it is decided to let the blade hang, so that it is self-balancing by the gravitational loading. By doing this, no pretension is needed to balance the system. Besides, due to centrifugal loads, the effect of the gravitational loading is minimal on a rotating helicopter blade.

Global blade dimensions

To be able to test the demonstrator with on-blade sensors, the blade should be sufficiently large. To test the characteristics of the demonstrator, a simple strip will be used instead of a blade-like profile for the first tests. This strip will have a constant thickness over the chord length and blade length. The chord length is chosen to be around 10% of the blade length, while the thickness will be around 1% of the blade length. To start the design process, the initial blade length was arbitrarily chosen to be 500mm. For later tests, blade profiles with comparable blade lengths can be used.

3.7 Summary

This chapter described the first phase of the design process. This last concluding section will give an overview of where the design process stands after this chapter.

The desired frequencies are set as follows:

$\Omega = 10\text{Hz}$	Controlled rotor frequency
$f_{l_r} = 0.3\Omega = 3\text{Hz}$	Restrained rotor/blade frequency
$f_{f_r} = 1.04\Omega = 10.4\text{Hz}$	Restrained rotor/blade frequency
$f_{f_{el,1}} = 2.68\Omega = 26.8\text{Hz}$	Restrained rotor/blade frequency

The pitch will be actuated at Ω, while the design of the flap and lag hinges will have to result in the other three frequencies.

The demonstrator will be actuated by two different excitation sources. Pitch will be actuated at a constant frequency Ω, while flap is to be actuated at a broadband frequency signal to mimic a more realistic situation for the helicopter blade. By having two independent excitation sources for the demonstrator, it can be placed in the 'empty' shaded quarter of table 2.4, with two DOFs being actuated independently and all being monitored.

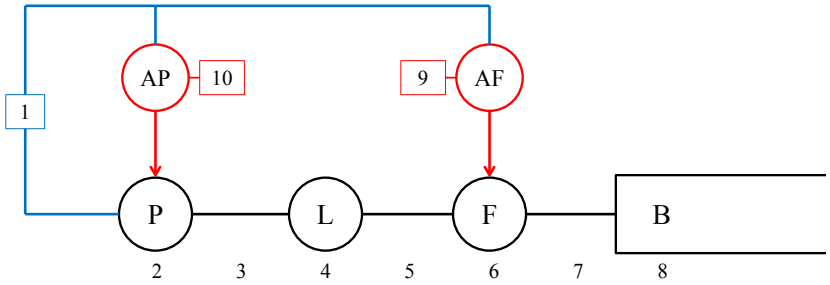

Figure 3.3: Schematic structure of the demonstrator

Figure 3.1 in section 3.3 showed the global structure of the demonstrator without actuation. Now that it is decided which DOFs are being actuated, a more detailed structure can be sketched. This updated structure is shown in figure 3.3. In this figure, the black subsystems form the actual demonstrator. The red parts represents the actuation sources, they are connected to the pitch and flap hinges. The blue part forms the frame in which the demonstrator will be mounted. As can be seen, ten subsections are identified:

1. Connecting frame
2. Pitch hinge
3. Pitch-lag connection
4. Lag hinge
5. Lag-flap connection
6. Flap hinge
7. Flap-blade connection
8. Blade
9. Actuation of flap
10. Actuation of pitch

4. Design of the demonstrator

The previous chapter described the first phase of the design process. This chapter will go into detail on the actual design of the demonstrator, i.e. the black subsystems of figure 3.3. The design process went from subsystem 8 to 2; the blade and its clamp were first designed, followed by the flap hinge, lag hinge and the pitch hinge. The modeling CAD software package SolidWorks was used for the design of the demonstrator. This chapter will first present the final design of the demonstrator, after which the design of the individual subsystems is described.

4.1 End result

The final design of the demonstrator is shown in figure 4.1. In this figure, the red dashed line represents the flap axis, the yellow one represents the lag axis and the black one represents the pitch axis.

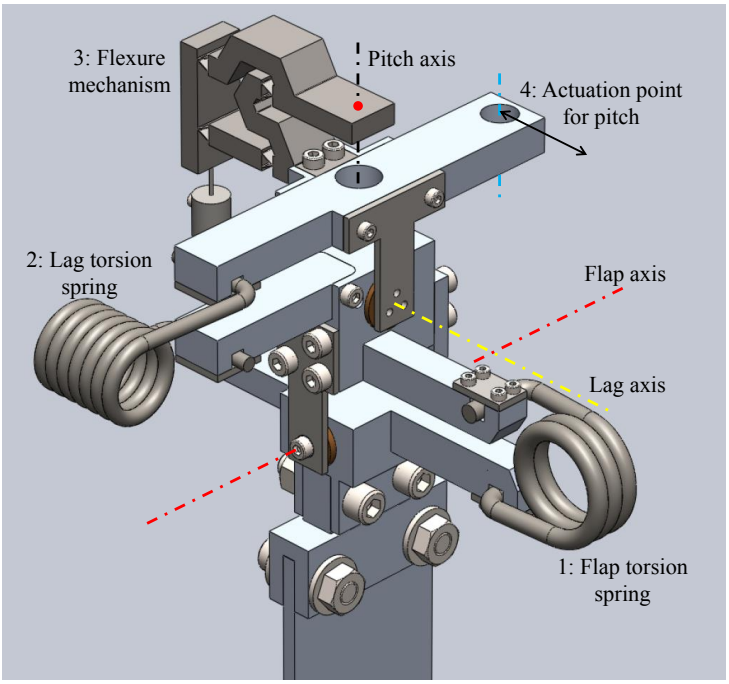

Figure 4.1: The final design of the demonstrator

The numbers in the figure represent the following:

1. Torsion spring that is used to generate a rotational stiffness in the flap hinge. The rotational stiffness is needed to realize the desired flapping frequencies for the blade. The selection of this torsion spring is described in section 4.3.

2. Torsion spring that is used to generate a rotational stiffness in the lag hinge, this is needed to realize the desired rigid body frequency for lag. The selection of this torsion spring is described in section 4.4.

3. Flexure mechanism that is used to be able to actuate flapping at a point that only rotates when pitch is actuated. Because of this flexure, the actuation source for flapping can be mounted in a non-moving environment, while exerting a force on a point that displays flap and lag. The red dot is the point where the flexure will be actuated, this point is located on the pitch axis, so it will only rotate along with pitch. The design of the flexure is described in section 5.1.

4. The point where pitch will be actuated. It is decided to actuate pitch with a translational actuator. The selection of an actuator is described in section 5.2.

4.2 Blade clamp

As stated in the design requirements, the demonstrator should be designed such that the blade can be easily replaced. This is required to be able to test different blade profiles with it. To make it possible to replace the blade easily, it is decided to use a blade clamp as a connecting part between the flap hinge and the blade. This part will be replaced with other blade configurations. The section that clamps the blade will change with other blade profiles, while the section that is connected to the flap hinge will have to be the same for all blade configurations.

Figure 4.2 shows the design of the blade clamp. The bottom section is the specific part where the blade will be clamped, this is the part that will change for different blade configurations. The design of this specific section depends on the blade profile that is used. The top section is the generic part that will be mounted in the flap hinge. This end section is 30mm wide, 10mm thick and 16mm high.

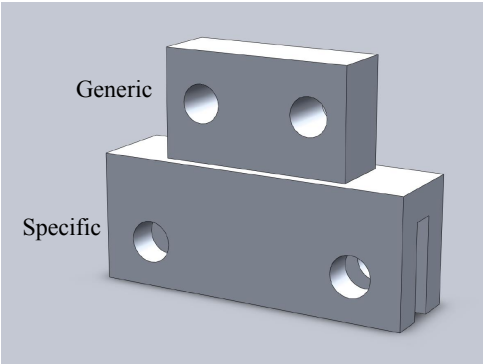

Figure 4.2: Design of the blade clamp

4.3 Flap hinge

This section describes the design of the flap hinge. At first, the design process of the hinge is explained, followed by the actual design of the hinge.

4.3.1 Design process

The design procedure that was presented in figure 3.2 contains a double arrow between the boxes 'Blade + Clamp' and 'K_{flap}'. This double arrow represents an iterative process, which will be explained into further detail.

The design requirements state that the ratios between the different mode frequencies of the demonstrator should give a representation of a real helicopter RBS; the rigid and the first elastic flapping mode frequencies should be in the same range with respect to the operation frequency Ω as they are in table 2.1. To realize the desired flapping frequencies, an added rotational stiffness is necessary in the flap hinge. The effect of this added rotational stiffness on the elastic body frequency of the blade is determined in appendix A. It appears that adding a rotational stiffness in the hinge leads to a decrease of the bending frequency, while increasing the rigid body frequency.

With the method described in the appendix, it is possible to calculate the elastic body frequency when the blade parameters and the rotational stiffness are known. To get both the rigid and elastic body frequencies in the range of the desired frequencies, the blade parameters can be changed. The iterative process of figure 3.2 is schematically shown in figure 4.3. For the initial blade design, the required rotational stiffness for the rigid flapping frequency is calculated. With the stiffness known, the resulting elastic flapping frequency is calculated using the method of appendix A. If this fulfills the design requirements, the required rotational stiffness is known and the flap hinge can be designed. If the result is not good enough, the parameters of the blade are changed until the requirements are fulfilled.

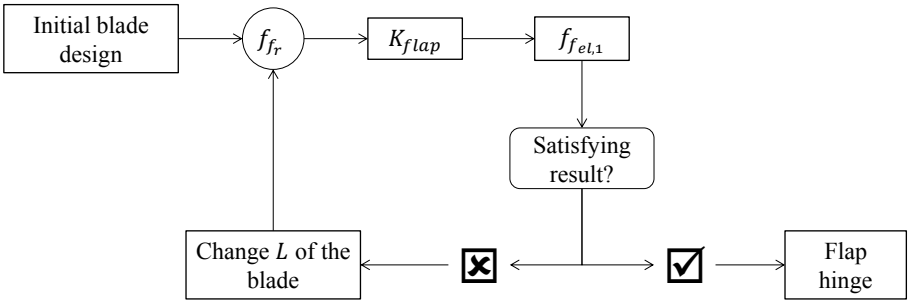

Figure 4.3: Iterative process to realize the desired frequencies

As can be seen in this figure, only the length of the blade was changed when the desired frequencies were not realized. This is done because the width of the blade does not have an effect on the natural frequencies, while it is favorable to use a standard thickness for the blade; a thickness of 4mm is used. Following this process, the required rotational stiffness and blade length were found to be $C_F \approx 2.2$Nm/deg and $L = 551$mm.

4.3.2 Hinge design

There are different ways to generate a rotational stiffness in the flap hinge. It can be done by placing a torsion spring directly on the flap axis. However, if small angles are assumed, the torsional stiffness can also be generated by placing a linear stiffness at a certain distance from the flap axis. See figure 4.4.

It is decided to generate the rotational stiffness by using an external stiffness at a certain distance from the flap hinge. When the rotational stiffness is generated at the outside of the system, it is easy to replace it when other blade configurations that require a different stiffness are used. Besides, when an external stiffness is used, it will be easier to control the distance between the hinges; a quick investigation of standard torsion springs that could be used shows that relatively large torsion springs are needed to realize the required rotational stiffness in the hinge. This automatically means that the hinge itself, and thus the distance between the flap and lag hinge, will become large as well. The distance between these hinges will quickly become around 15 to 20% of the blade length. This is highly unfavorable; the different axes are all close to the root in a fully articulated helicopter rotor, so to better represent a helicopter RBS, it is favorable to keep the distance between the hinges as small as possible.

The solution that was eventually used involves a torsion spring that is located outside the hinges. The spring that is used for this is connected to the flap hinge at one end and the lag hinge at the other end. It was ordered at Lesjöfors, a spring supplier company that produces and supplies a large selection of

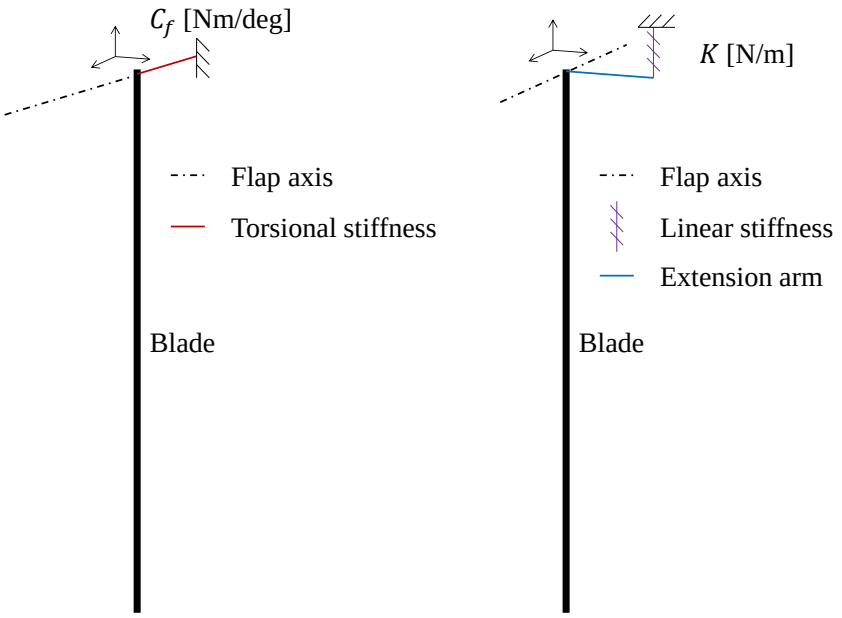

Figure 4.4: Two ways to generate a rotational stiffness in the hinge

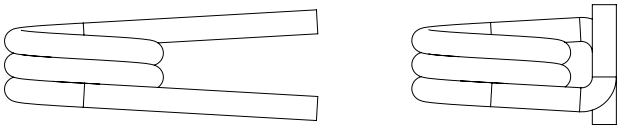

Figure 4.5: Torsion spring end design

standard springs, including torsion springs [29]. It was possible to customize the design of the standard springs to be able to fit them in the design. For the spring that was selected for the flap hinge, the leg length was changed. Besides, the springs' end design was customized to be able to fit it more easily in the design, see figure 4.5. The legs of the left spring are in the original configuration, while the right one has the customized configuration that is used in the demonstrator.

The torsion spring that was used for the flap hinge is a customized SF-VFR 8503, with a spring rate of 0.488Nm/deg [29]. The arm that was used to connect the torsion spring was arbitrarily chosen to be 50mm. With these parameters, the leg length that was required to realize a rotational stiffness of $C_F \approx 2.2$Nm/deg was calculated to be 23.5mm. The derivation of this required leg length is explained in appendix B.

At this stage of the design process of the flap hinge, it is known how the torsion spring is going to be implemented in the hinge. Besides, the hinge should contain a clamping section to connect the blade. These are the two most important characteristics of the hinge, so the rest of the design of the hinge can now be done. Figure 4.6 shows the final design of the flap hinge. The bottom section is the part that clamps the blade, the black dashed line is the flap axis and the arm in the front is the part where the torsion spring is connected.

With the blade, the clamp and the flap hinge designed, the design of the first subsystems of the demonstrator is finished. Figure 4.7 shows the assembly as it is at this stage of the design process. The end of the torsion spring that is not connected to anything will form a connection to the lag hinge.

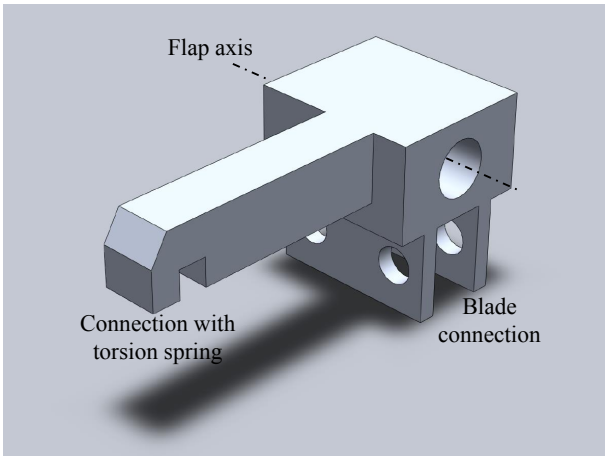

Figure 4.6: Design of the flap hinge

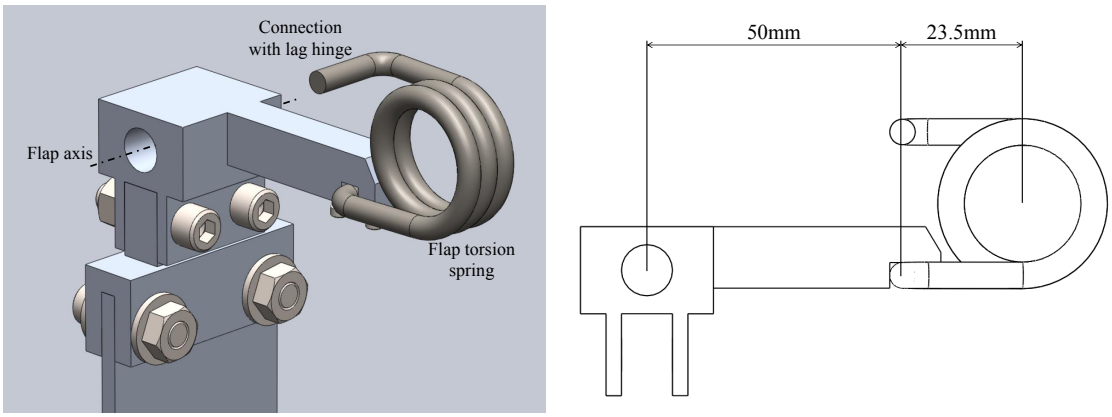

Figure 4.7: Assembly of subsystems 6 to 8

4.4 Lag hinge

Following the procedure of figure 3.2, the design of the lag hinge is next in the process. This section will describe the design of this hinge. The following requirements are made for the design:

- Form a connection with the flap torsion spring
- Form a connection to the flap axis, while releasing the flapping motion of the flap hinge
- Generate a rotational stiffness that results in a rigid lagging frequency of $f_{l_r} \approx 3$Hz

When looking at the schematic structure of the demonstrator in figure 3.3, the subsystems 6, 7 and 8 are already designed at this stage. Because these parts will all display lag in the demonstrator, they should be taken into account to be able to calculate the required rotational stiffness of the lag hinge. It is desired to have the lag and the flap axes close to each other, to generate a more realistic representation of a helicopter rotor. For this reason, it is decided to make use of an external torsion spring for the lag hinge as well.

A global design of the lag hinge was made to set a distance between the flap and lag axes. With this global design, the torsional stiffness that is required to realize the rigid lagging frequency is calculated to be $C_L \approx 0.19$Nm/deg. A SF-VFR 8480 torsion spring of Lesjöfors was selected to be used for the lag hinge. This spring has a spring rate of 0.103Nm/deg [29]. As for the torsion spring that was used in the flap hinge, the legs of the spring were customized to fit more easily in the design. Besides, the required

leg length was calculated with the method of appendix B, this turned out to be 36.4mm with an arm of 50mm for the lag axis.

The design of the lag hinge is shown in figure 4.8. As can be seen, the hinge has two arms. The bottom one is the arm that connects to the torsion spring of the flap hinge, while the top one connects to the lag torsion spring. To ease the manufacturing process of the lag hinge, it will be made out of two pieces. The arm that is connected to the lag torsion spring will be made as a separate part and will be mounted to the rest of the hinge by bolts.

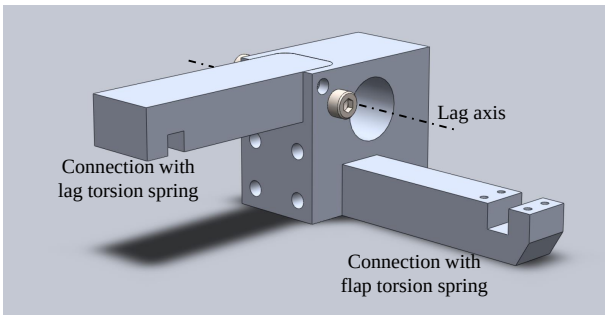

Figure 4.8: Design of the lag hinge

With the lag hinge designed, the assembly can be updated to a system where subsystems 4 to 8 are present. This updated assembly is shown in figure 4.9. The flap hinge is made transparent in this figure, to clarify how the flap and lag hinges are connected to each other. As can be seen, the flap shaft is connected to the lag hinge. The flapping motion is released by two standard plain bearings between the flap shaft and the hinge. The parts used for this are standard bronze plain bearings (GLI BBF 061010) that are ordered at Brammer [30]. The numbers in the figure indicate the following:

1. Flap axis
2. Flap torsion spring
3. Plain bearings used to release flapping motion between the flap hinge and shaft
4. Lag axis
5. Lag torsion spring
6. Connection with pitch hinge

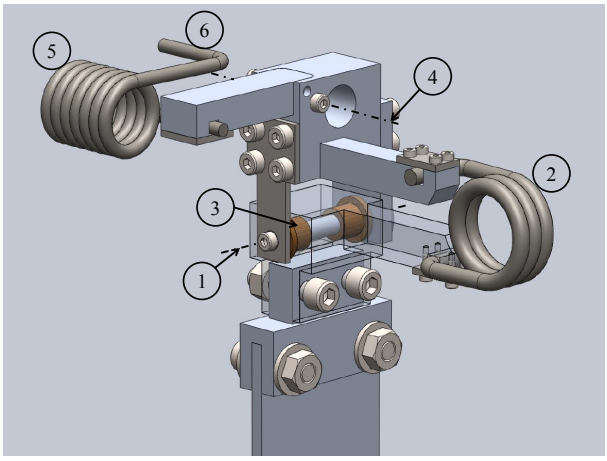

Figure 4.9: Assembly of subsystems 4 to 8

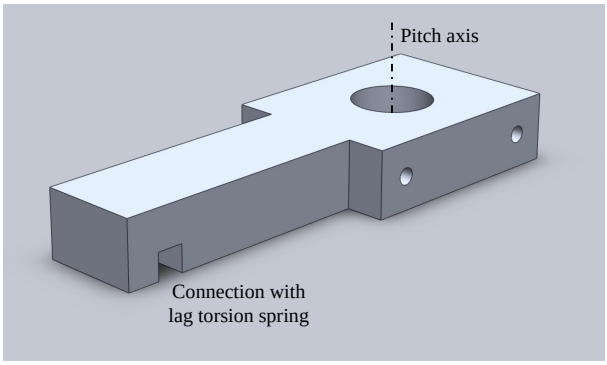

Figure 4.10: Design of the pitch hinge

4.5 Pitch hinge

At this stage of the design process, the blade, the flap hinge and the lag hinge are all designed. The torsion spring of the lag hinge has to be connected to the next hinge, i.e. the pitch hinge. This section describes the design process of this last hinge. This is the least complex of the three hinges, because it has no constraints for mode frequencies. The three desired frequencies f_{l_r}, f_{f_r} and $f_{f_{el,1}}$ are all constraint by the flap and lag hinges, while the frequency corresponding to pitch will be actuated at the operation frequency.

The requirements for the pitch hinge are listed as follows:

- Connect to the lag torsion spring
- Form a connection with the lag axis, while releasing the lagging motion of the lag hinge

The design of the pitch hinge is shown in figure 4.10. The arm in the front of this figure will be connected to the lag torsion spring. The threaded holes on both sides are to mount the connection plates to the sides. These plates are made out of 2mm thick steel and will be made by laser cutting. They are used to connect the pitch hinge to the lag shaft.

With the pitch hinge designed, the assembly of subsystems 2 to 8 can be made. This updated assembly is shown in figure 4.11. The lagging motion is released by a plain bearing between the lag shaft and the lag hinge. This is shown in figure 4.12. This figure shows the section view of the rectangular area in figure 4.11. The bearing that is used for this, is a standard bronze plain bearing (GLI BBF 101320) that is ordered at Brammer [30]. The numbers in the figure indicate the following:

1. Lag axis
2. Plain bearing that is used to release lagging motion between the lag hinge and shaft
3. Lag shaft
4. Pitch axis

4.6 Summary

This chapter described the design of the structure of the demonstrator. At this stage, the demonstrator is designed such that the three DOFs are released and the desired mode frequencies are realized. The operation frequency should be realized by the actuation of pitch.

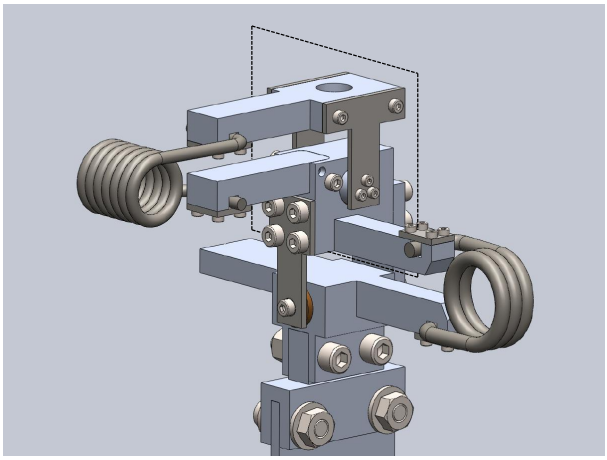

Figure 4.11: Assembly of subsystems 2 to 8

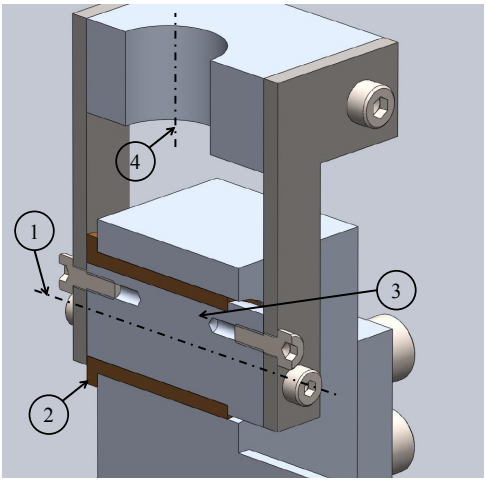

Figure 4.12: Section view of the connection to the lag hinge

Looking back at figure 3.3, the black part, i.e. subsystems 2 to 8, is designed at this stage. The remaining subsystems, i.e. the actuation and the frame, should still be designed. The design of these subsystems is described in the next chapter.

5. Design of actuation and frame

The previous chapter described the design of the demonstrator. So far, only the black subsystems of figure 3.3 are designed. The system should however also be actuated. Section 3.3 already mentioned actuation of the system. It was concluded that pitch should be actuated at a constant frequency Ω, while flap should be actuated with a broadband frequency signal to generate a more realistic representation of a helicopter RBS. The design of the actuation of the demonstrator is described in this chapter. Besides, the design of the frame is presented at the end of this chapter.

5.1 Actuation of flap

To realize actuation at a broadband frequency signal, it is decided to excite flap with a shaker. A B&K Mini Shaker Type 4810 is available at the chair of Applied Mechanics, so to prevent unnecessary expenses, it is decided to use this shaker to excite flap. The data sheet of this type of shaker is presented in appendix D.

When looking at the structure of the demonstrator, one can conclude that actuation of flap can become a complex procedure when pitch and lag are also active. Because of these active modes, there is no non-moving point on the flap hinge where flap can easily be excited, so this will have to be done on a moving point of excitation. A possible solution to excite flap in combination with pitch is to let the excitation source, i.e. the shaker, move with pitch as well. However, by doing this, the relatively large moving mass of the shaker will have a large influence on the total inertia of the system, which can lead to instabilities. Besides, a much stronger excitation source for the pitch will be needed. For these reasons, it is decided to make the design such that the shaker can be located at a fixed position.

With the excitation source fixed, the output of it should still be able to reach a moving point, i.e. the flap hinge. The solution for this was found in a flexible element that was specially designed for the demonstrator. This flexure is made out of a single piece of material and contains multiple flexible sections. It is manufactured by Electric Discharge Machining (EDM), a manufacturing process that uses electrical discharge sparks to remove material [31]. The design and analysis of this flexure will be described in this section.

5.1.1 Design of the flexure

The goal of the flexure is to translate the vertical movement actuated by the non-moving shaker to the moving flap hinge. If the shaker would actuate the flexure on a point located on the pitch axis, this point would not display any horizontal displacement; the point will only rotate along with pitch. The vertical displacement actuated by the shaker should however be transferred to a point on the moving flap hinge. This is done by making use of a so called four bar linkage, where the opposite bars are always parallel with respect to each other. The initial design of the flexure is shown in figure 5.1. The numbers in the figure represent the following:

1. Input point; the point where the flexure will be actuated. This point is located on the axis of rotation for pitch.

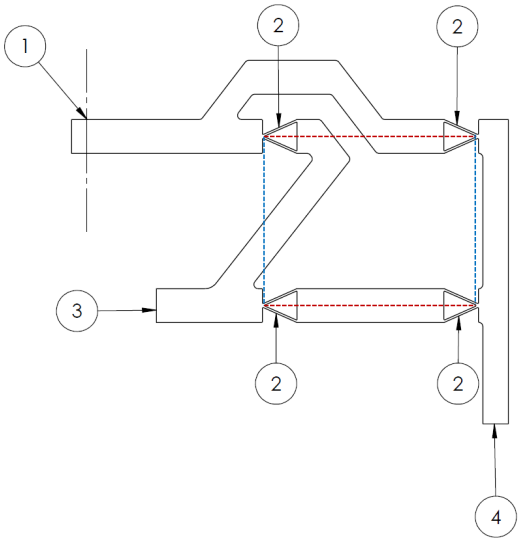

Figure 5.1: Initial design of the flexure

2. Flexible hinges
3. Point where the flexure will be connected to the pitch hinge
4. Output point; the point where the flexure will be connected to the flap hinge

The four flexible hinges in the element form the four bar linkage; the box formed by the blue and red dashed lines is able to deform as a parallelogram. When a downwards force is subjected to the flexure at 1, this results in an upwards movement at 4, where the flexure will be connected to an extension of the flap hinge. This means that a downwards force at 1 generates a moment around the flap axis.

Each of the flexible hinges is formed by two leafs, thin pieces of material that are easy to deform. The hinges are shaped triangular, the triangular shape is formed by two leafs per hinge. Other options would be to use only one leaf per hinge, however, this was not favorable for the flexure; if the leafs would be placed horizontally, they would experience large shear loadings, while vertical placed leafs might experience problems with buckling. Besides, the flexure would easily deform by torsion of the vertical leafs when pitch is actuated, which is an unwanted deformation of the flexure. With the triangular shape, the hinges have a higher resistance against buckling, shear and torsional loadings, so this is judged to be the best implementation of creating a flexible hinge for the flexure.

5.1.2 Analysis of the flexure

The flexure was analyzed with the finite element simulation software ANSYS to come up with the detailed design. The model in ANSYS was built up by a combination of beam and shell elements. The leafs were modeled as shells, while the rest of the element was modeled as beams. A spring was subjected to the flexure's end, to model the effect of the torsional stiffness of the flap hinge. A detailed description of the ANSYS model is given in appendix C.

The initial design was modeled in ANSYS. A modal analysis was performed to determine the first number of mode shapes and their corresponding frequencies. This first analysis resulted in many low frequent modes, which is not favorable.

By changing the different design parameters, the characteristics of the mechanism were improved. There is only one wanted mode, i.e. the mode where the leafs of the hinges deform by bending. It is preferable that the frequency corresponding to this mode is low, so that it is easy to excite it. The frequencies corresponding to the other modes are preferably high.

Five design parameters were varied to determine their effect on the mode frequencies; i.e. the leaf thickness, the height of the beams between the hinges, the height of a single leaf, the length of a single hinge and the width of the total mechanism. These different design parameters are shown in figure 5.2. A first analysis that was used as reference was performed. With respect to this reference analysis, one parameter was changed every time to determine the effect of an increase or decrease of that specific parameter. Table 5.1 displays the values of the first five mode frequencies for the six analyses. The first test was the reference, for the other five tests, the bold value is the parameter that was changed with respect to the reference analysis.

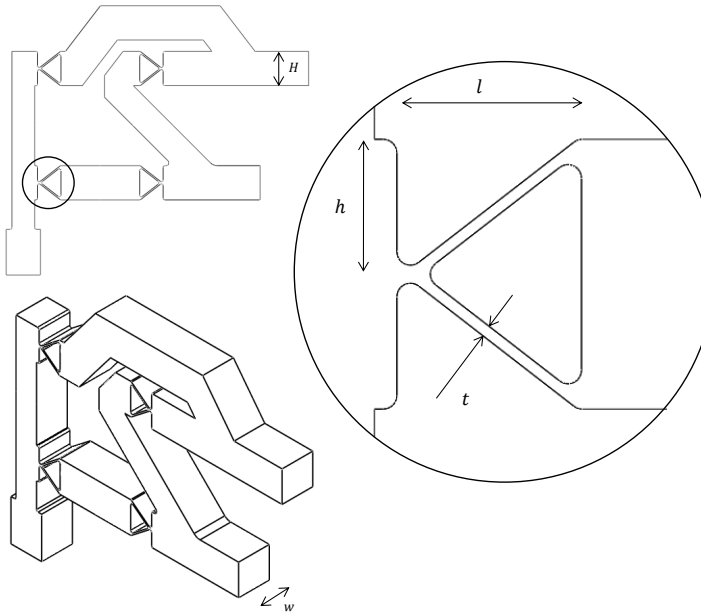

Figure 5.2: Design parameters of the flexure

Table 5.1: The effect of different design parameters on the first five mode frequencies of the flexure, dimensions in mm

Mode #	t0.25, H4, h2, l4, w5	**t0.4**, H4, h2 l4, w5	t0.25, **H8**, h2, l4, w5	t0.25, H4, **h4**, l4 w5	t0.25, H4, h2, **l7**, w5	t0.25, H4, h2, l4, **w10**
1	1.21Hz	2.37Hz	1.21Hz	0.98Hz	1.02Hz	1.29Hz
2	5.26Hz	5.84Hz	7.21Hz	4.02Hz	5.38Hz	7.07Hz
3	10.13Hz	11.25Hz	13.17Hz	9.35Hz	9.25Hz	13.49Hz
4	13.42Hz	13.67Hz	18.84Hz	12.04Hz	12.99Hz	21.62Hz
5	16.76Hz	17.92Hz	34.70Hz	15.27Hz	16.40Hz	26.18Hz

For each of the tests, the first mode was the wanted mode where the flexure deforms by pure bending of the leafs. The second mode is described by rotation around the vertical axis caused by torsional bending of the leafs. This second mode is highly unwanted at low frequencies, since it will be activated by actuation of pitch.

When looking at the table, the following conclusions can be drawn regarding the effect of the different parameters on the mode frequencies:

1. An increase in leaf thickness increases the first mode frequency. Other modes are not that much affected. Regarding the first mode, this effect is expected, since the bending stiffness of the leaf changes in directly proportion with the area moment of inertia of the leaf, which has the leaf thickness to the third power in it: $I = \frac{1}{12}wt^3$. The second mode seems to be a mode that is described as a combination of torsional bending of the leafs and beams. The torsional stiffness of

the leafs depend on the polar area moment of inertia: $J = \frac{1}{12}\left(wt^3 + w^3t\right) \approx \frac{1}{12}w^3t$. This shows why the second mode does not change that much when the thickness is increased.

2. An increase in beam height does not affect the first mode frequency, it does however increase the unwanted mode frequencies. This is explained by the fact that an increase in beam height will result in an increase in bending and torsional stiffness of the beams. The first mode does not depend on the beam bending stiffness, so that explains why it is not affected by an increase in the beam height.

3. An increase in the leaf height results in a decrease in all mode frequencies. Because the flexible length of the leafs increases, the bending and torsional stiffness will both decrease. This explains the relatively large decrease of the first two mode frequencies. The decrease of the second mode frequency can also be explained by the change of the angle of the leafs. The leafs are more vertically oriented when the leaf height increases, which makes it easier to realize rotation around the vertical axis by torsional bending and as mentioned, the second mode is described as rotation around the vertical axis.

4. When the hinge length is increased, the first mode frequency is decreased. The rest of the modes experience a small increase or decrease for their frequency. As for the leaf height, the decrease of the first mode frequency is explained by the fact that the flexible length of the leaf increases. The second mode frequency however does not decrease. This is explained by the angle of the leafs and the mode shape. The leafs are more horizontally oriented when the hinge length is increased, which makes it more stiff for rotation around the vertical axis.

5. An increase in the total width of the flexure results in an increase in the unwanted mode frequencies. The first mode frequency experiences a relatively small increase. For the first two modes, this is explained by the fact that the bending stiffness of the leafs increases with the same factor as the width, while the torsional stiffness increases with the factor to the third power.

5.1.3 Final design

With the conclusions of the parameter tests performed in ANSYS, an improved design of the flexure mechanism was designed. It was advised to use titanium grade 5 for the flexure. Furthermore, the minimum applicable leaf thickness is 0.2mm and to prevent fatigue, it is advised to keep the maximum stress in the system below one third of the material's yield stress [32].

The leaf thickness, beam height and the total width of the system were the parameters that were changed with respect to the first analysis. The leaf thickness was decreased to the minimum possible thickness, i.e. 0.2mm. Furthermore, the beam height was set to 6mm and the flexure's width was increased to 15mm. The hinge length and height were unchanged with respect to the reference analysis. Even though an increase in hinge length had a positive effect on the mode frequencies, this parameter was not changed. This is done because an increase in length would result in more horizontally oriented leafs; they would be loaded more in shear, which is unwanted. With the changed parameters, the first mode frequency remains relatively low (1.69Hz), while the frequencies of the unwanted modes are all increased. The first unwanted mode is shifted to 14.1Hz.

Besides the mode frequencies of the mechanism, it is important to consider the maximum stress that would be present in the system. The selected shaker for the actuation of flap can exert a force up to 10N. To determine the maximum stress in the system, a static analysis was performed with a force of 10N on the flexure. The stress distribution of the flexure in shown in figure 5.3, the maximum stress was found to be 76MPa and was located at the point where the leafs come together. Titanium grade 5 shows an endurance limit around 240MPa [33], so it is not likely that the flexure will experience problems with fatigue. The maximum deflection at this 10N force was 0.22mm, which corresponds with a flapping angle of 0.25°. This is a relatively small angle, however, because it was experienced to be difficult to get realize satisfying mode frequencies, it is decided to go with this design and thus work with small flapping angles. The final design of the flexure is shown in figure 5.4.

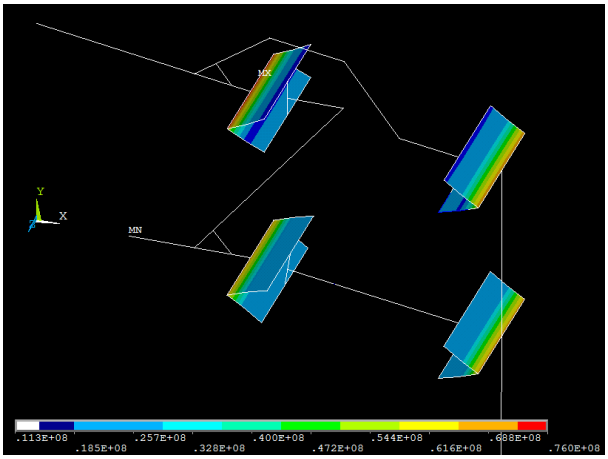

Figure 5.3: Stress distribution in the flexure

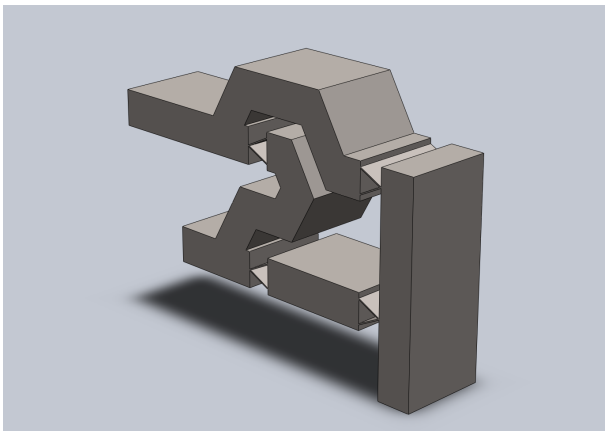

Figure 5.4: The final design of the flexure

5.1.4 Implementation in the demonstrator

With the flexure designed, it is possible to generate a moment around the flap axis while keeping the flap excitation source on the pitch axis. The flexure is however only designed to translate a vertical force. It cannot be directly connected to the flap hinge, since it is not able to display a flap or lag angle, while the flap axis will be flapping and lagging. In other words, the two should be connected in a way that they are possible to display flap and lag with respect to each other. This is done by two sprits with a small diameter that are mounted in a tube, see figure 5.5. The sprits will be able to deform by bending, so that the blade can display flap and lag without generating too much internal stresses in the flexure.

To connect the flexure to the pitch hinge, a new part is designed that connects the lag and pitch hinge with each other. This new part has an increased thickness, so that thread can be tapped in it and the flexure can be mounted to it. Figure 5.6 shows how the flexure is implemented in the demonstrator assembly. The three axes of rotation for flap, lag and pitch are shown as dashed lines in this figure.

5.2 Actuation of pitch

The previous section described the design of the actuation of flapping. This section will describe the design of the other actuation source, i.e. actuation of pitch. First, it is decided how the pitch is going to be actuated, followed by the actual selection of an actuator.

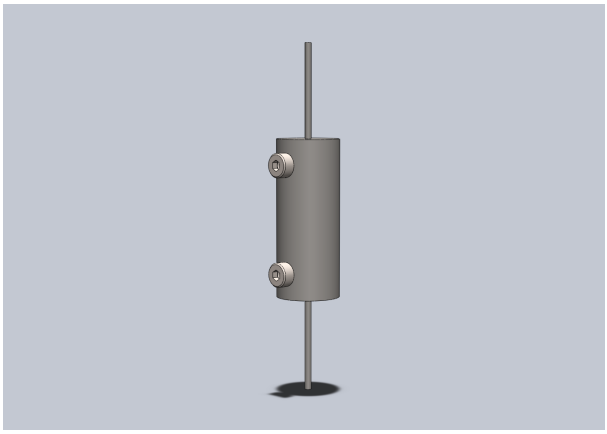

Figure 5.5: Implementation of the flexure in the demonstrator

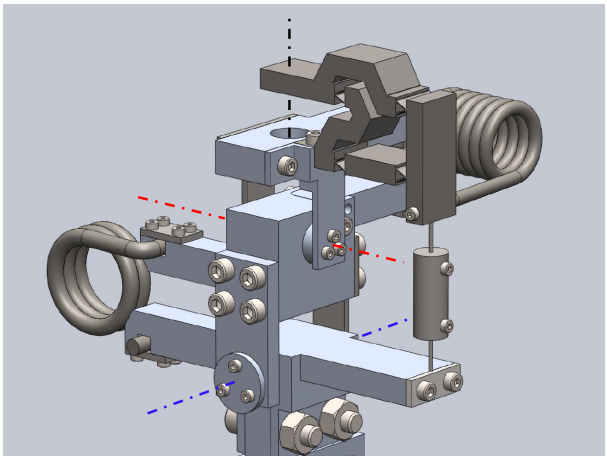

Figure 5.6: Implementation of the flexure in the demonstrator

5.2.1 Type of actuator

For the actuation of cyclic pitch, an actuator that excites at a constant frequency should be chosen. Two types of actuation are possible; torsional and translational actuation. A torsional actuator could have its output on the pitch axis, while a translational actuator should have its output at a distance r from the pitch axis to be able to generate a moment.

Since flap will be actuated with a shaker that is located on the pitch axis, it becomes complex to include torsional actuation with the actuator on the pitch axis. This means that the advantage of actuating directly on the pitch axis is lost. For this reason, it is decided to select a translational actuator to actuate cyclic pitch.

5.2.2 Selection of an actuator

For the selection of a suitable actuator, a SolidWorks model of the demonstrator was used to determine the mass moment of inertia I_y with respect to the pitch axis. For the first calculations, it was decided to work with an arm of $r = 50$mm for the actuation and an angle amplitude of $\Theta = 5°$. The total stroke for the actuator is $X \approx 2\Theta r = 8.7$mm (from $+\Theta$ to $-\Theta$). Since this total distance is relatively small, the actuator that will be selected is required to have little play.

With the operation frequency being $\Omega = 10\text{Hz} = 20\pi\text{rad}$, the output function for the actuation becomes $x(t) = \Theta r \sin \Omega t$. With this function for the actuation, the maximum velocity, acceleration and force are

calculated:

$$\dot{x}_{max} = \Omega\Theta r = 0.55\text{m/s} \tag{5.1}$$

$$\ddot{x}_{max} = \Omega^2\Theta r = 34.5\text{m/s}^2 \tag{5.2}$$

$$F_{max} = m_{eff}\ddot{x}_{max} = 11.7\text{N}, \tag{5.3}$$

where m_{eff} is the effective moving mass of the demonstrator experienced by the actuator:

$$m_{eff} = I_y/r^2 = 0.34\text{kg} \tag{5.4}$$

To reduce play and backlash between the cycles, it was decided to select a Voice Coil Motor (VCM). A VCM is an actuator that consists of two separate parts, i.e. the magnetic core and the coil. Applying a voltage to the coil will result in a motion in one direction. Reversing the polarity of the voltage will result in a motion in the opposite direction [34]. VCMs allow fast acceleration and high speed operations and do not display backlash when the direction of the force is changed. For these reasons, a VCM seems suitable to be used to actuate cyclic pitch.

To select the right VCM, the Root Mean Square (RMS) of the force had to be calculated. For a sinusoidal profile, which will be the case for the demonstrator, the RMS of the force can be calculated as follows [35]:

$$F_{RMS} = \frac{13.8mX}{T^2}, \tag{5.5}$$

where m is the total moving mass (mass of the moving coil plus the effective moving mass of the demonstrator) and T is the time of one cycle. The F_{RMS} should be less than the continuous force F_C of the selected motor. Besides the RMS of the force, the RMS of the current in ampere, I_{RMS}, is an important parameter to calculate. This parameter is used to calculate the power dissipation P, which should be less than the maximum continuous power P_C of the selected motor. For the sinusoidal profile, these parameters are calculated as follows:

$$I_{RMS} = \frac{13.8mX}{K_f T^2} \tag{5.6}$$

$$P = RI_{RMS}^2 \tag{5.7}$$

where K_f is the force constant of the motor in N/A and R is the resistance of the motor in Ohm.

Since the values of F_{RMS}, I_{RMS} and P all depend on the type of VCM that is to be chosen, the selection of a motor that fulfills the demands is a trial and error process. To prevent unnecessary expenses, it was investigated if a suitable VCM was available at the university. It was possible to use an AVM30-15 that was available at the chair of Mechanical Automation. After investigating this type of VCM, it was concluded that it was suitable to use it if the angle amplitude was reduced from $\Theta = 5°$ to $\Theta = 3°$. This change in angle amplitude is relatively large, i.e. a decrease of 40%. However, if this VCM turns out to function properly for the actuation of pitch and the angle is judged to be too small, it can be decided to order a different VCM that is able to actuate pitch with a larger amplitude. The data sheet of the selected VCM is presented in appendix E.

5.3 Frame

At this stage of the design process, the demonstrator is fully designed. The only thing left is the design of a frame that connects the demonstrator, the actuation sources and the rigid world with each other. The following requirements are listed for the design of the frame:

- Release pitch motion between the demonstrator and frame

- Connection with the VCM
  - Mount the core to the frame
  - Connect the coil to the pitch hinge
- Connection with the shaker
  - Suspend the shaker in the frame
  - Connect the shaker with the flexure on the pitch axis

End result

The final design of the demonstrator with the surrounding frame is shown in figure 5.7. A more detailed image is shown in figure 5.8. This figure shows the section where the demonstrator and the frame are connected into more detail. The numbers in this figure represent the following:

1. Mounting box in which the demonstrator will be hanged
2. Axial ball joint that connects with the shaker: standard part K0715 ordered from KIPP [36]
3. Connection between the VCM and the frame
4. Connection between the mounting box and the frame
5. Frame that connects the whole system with the rigid world

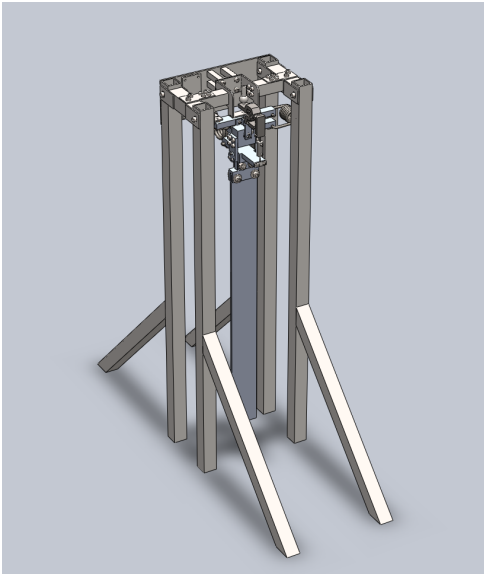

Figure 5.7: Design of the demonstrator and frame

Mounting box

The mounting box that will be used to suspend the demonstrator will be made from four 2mm thick steel plates that will be lasercut and welded to each other. It will form bolted connections with the frame and the demonstrator.

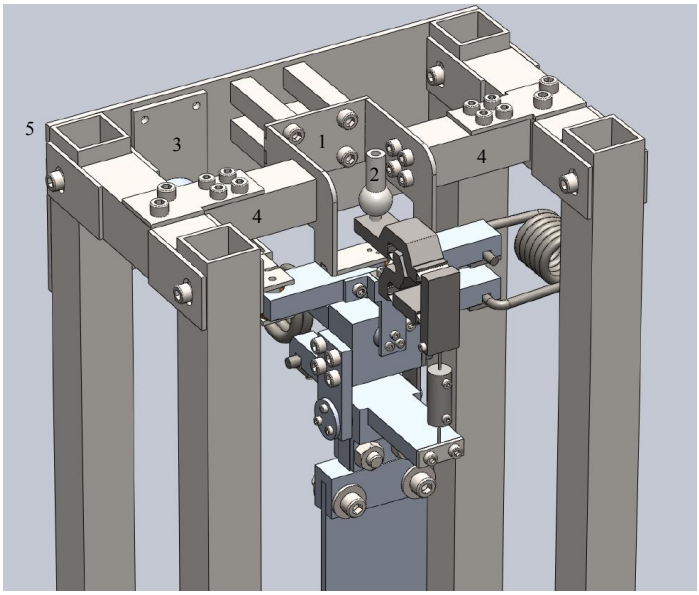

Figure 5.8: Connection between the demonstrator and frame

VCM connection

The VCM consists of two loose parts; the core and the coil. The coil will be the moving part and will have to be connected to the pitch hinge, while the core will not move and will have to be connected to the frame. Figure 5.9 shows how the VCM is implemented in the system. The numbers in the figure represent the following:

1. Pitch hinge
2. Connection between pitch hinge and VCM
3. VCM
   (a) Core (non-moving)
   (b) Coil (moving)
4. Plate that will be mounted to the back of the frame. The VCM is mounted to this plate as well.

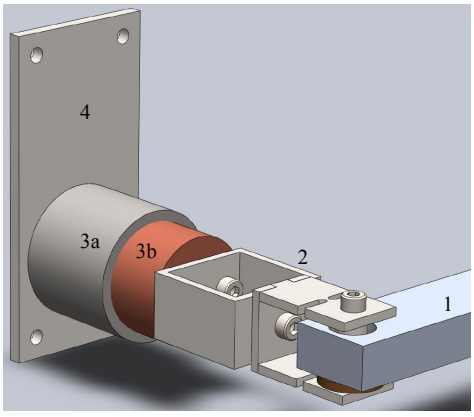

Figure 5.9: Connection between the frame, the VCM and the pitch hinge

Connecting frame

The frame that forms the connection with the rigid world is made out of steel 25x25x2mm tubes. To generate extra stability, they are supported by tubes that are cut at a 45 degree angle and are welded to the frame. To be able to mount everything to each other while keeping some freedom to disassemble the system, it is decided to make use of friction drilling. This is a method to make a hole in a thin walled structure without losing material. The material is plastically deformed to create more depth than the initial wall thickness [37]. Because of this extra depth, it is possible to tap thread in the tubes, so that the frame can be connected by bolts.

Shaker

To reduce the total height of the frame, it is decided to leave the shaker out of the frame. Instead, the shaker will be suspended in a different frame that will be built around the current frame. By doing this, the size of the frame can be significantly smaller than it would be when the shaker is implemented in the frame. Besides, it will be more easy to use a different size of shaker when kept out of the frame.

6. Experiments

The previous chapters described the design process of the demonstrator. After manufacturing the different parts and receiving the standard parts, experiments were performed to validate the design of the system. The following tests are performed:

- Flexure tests
  - Impact test to determine the mode frequencies
  - Static test to determine the stiffness
- Demonstrator tests
  - Excitation of flap with shaker
  - Impact flapping test
  - Manual lagging test
- Blade + flap hinge tests
  - Pendulum impact test
  - Impact test with the torsion spring connected
- Demonstrator double excitation test

The flexure tests were performed to conclude on the design of the mechanism in ANSYS. After these tests, tests with the demonstrator were performed to determine the flapping and lagging mode frequencies of the total assembly. Because these tests did not return the expected flapping mode frequencies, the blade and the flap hinge were tested separately from the system, to determine the effect of the external torsion spring on the flapping frequencies of the blade. The last test that was performed was to actuate both flap and pitch.

6.1 Flexure tests

Before assembling the total system, the flexure mechanism was tested to verify the ANSYS model. Two types of tests were performed for this part, a modal impact analysis was performed to determine the mode frequencies of the flexure and a static test was performed to determine its stiffness. This section describes the tests that were done with the flexure.

6.1.1 Modal analysis

The modal analysis was performed by clamping the flexure on a solid block, see figure 6.1 for a schematic overview of the setup. Goal of the impact test was to determine the different mode frequencies of the flexure and validate the ANSYS model.

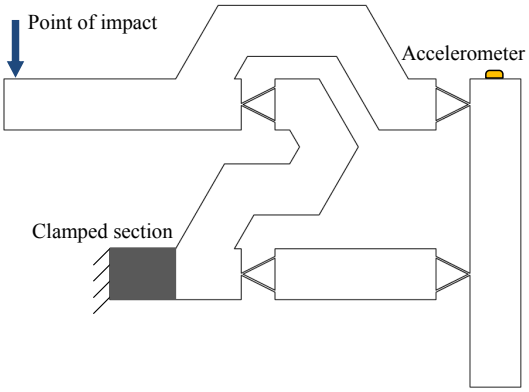

Figure 6.1: Setup for the flexure tests

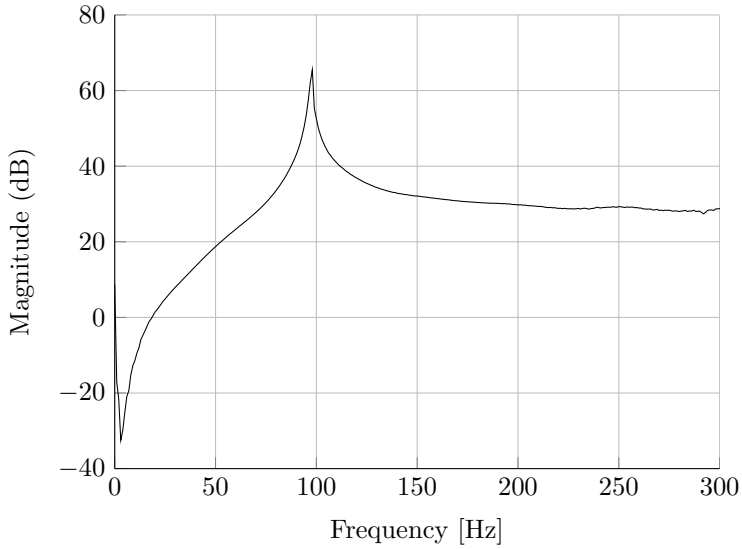

Figure 6.2: FRF of the impact test

The resulting Frequency-Response-Function (FRF) of the impact test is shown in figure 6.2. As can be seen, the first mode frequency determined by the impact test was found to be 97.5Hz, which is significantly higher than the first mode frequency found in ANSYS (≈1Hz for only the flexure).

6.1.2 Static tests

To find out the reason for the large difference between the predicted and the measured mode frequency, static tests were performed to determine the stiffness of the flexure. A constant load was subjected to the flexure by putting different weights on its end, while the deflection of the other end was measured by a deflection meter. The setup for the static tests is shown in figure 6.3.

Three different weights were used for the static tests: 100g, 200g and 500g. This method cannot determine the stiffness exactly, but the order of the stiffness can be determined by these tests. By doing this, a conclusion can be drawn about the static ANSYS analysis. The measured deflections for the different weights are listed in table 6.1. The tests indicate a deflection for the flexure of around 0,07mm/N. In ANSYS, when a force of 1N is subjected to the flexure's end, it results in a deflection of 0.055mm. This indicates that the order of the predicted stiffness in ANSYS is correct, so this is not the reason for the large error between the ANSYS model and the flexure.

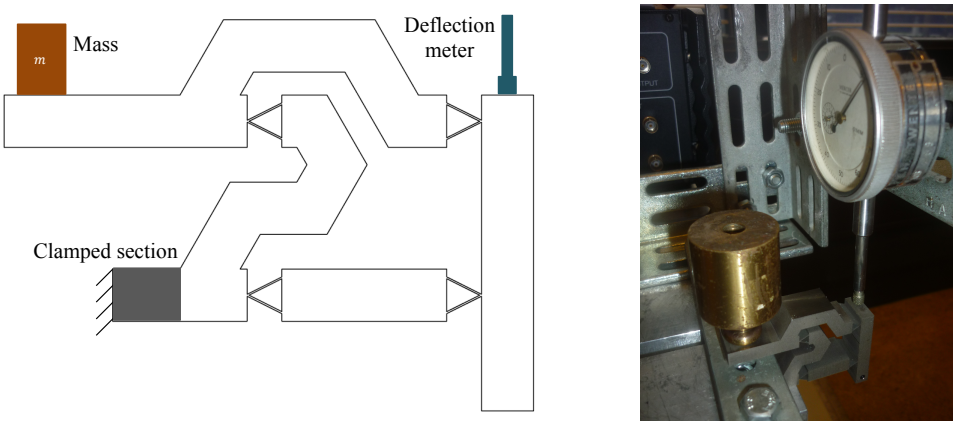

Figure 6.3: Static testing of the flexure

Table 6.1: Static tests of the flexure

Weight (g)	Deflection (mm)
100	0,07
200	0,14
500	0,37

6.1.3 Investigation of the ANSYS model

Since the cause of the problem of the error between the model and the flexure is not in the predicted stiffness, the ANSYS model is further investigated to find out what does cause this error. When looking at the standard formula for the natural frequency of a mass-spring system $\left(f_n = \sqrt{\frac{k}{m}}\right)$, it is likely that the error is caused by a (large) difference in mass between the ANSYS model and the flexure. For this reason, the mass summary of the ANSYS model was made and investigated. It turned out that the mass of the rigid beam elements (MPC184) was highly overestimated; the total mass of these elements combined was 868kg.

The rigid elements were used to connect the shell and beam elements with each other. To reduce their effect, they were given a cross section of 0,5x0,5mm in the original analysis. Investigation on the MPC184 element reference showed that the cross-sectional area of the element is set to unity [38]. In other words, the prescribed cross-sectional area of 0,25mm^2 for these elements is overwritten by ANSYS to 1m^2.

A new ANSYS analysis was performed, where the rigid beam elements were meshed with a different material with a negligible density ($\rho = 0.001$kg/m^3). By doing this, the total mass sum of the rigid elements can be neglected in comparison with the mass of the beam elements, despite having a cross-sectional area of 1m^2. This new analysis resulted in a frequency of 127.5Hz for the first mode, while the second mode was not found to be below 1000Hz. This new found first mode frequency is significantly more accurate than the frequency found in the original analysis.

Due to the error in the ANSYS analysis, the mode frequencies were highly underestimated. This means that the stiffness of the flexure could have been significantly lower without the unwanted modes becoming a problem. With the frequency corresponding to the wanted mode of the flexure being close to 100Hz, it is not in the range of the interesting frequencies for the demonstrator; i.e. from 0 to 30Hz, so more effort is needed to use the flexure's first mode.

6.2 Demonstrator tests

After the static and modal analyses of the flexure were performed, it was assembled in the demonstrator, so that the full assembly could be tested. The demonstrator was designed such that both flap and pitch could be excited. However, to be able to determine the flapping frequencies more easily, it was decided to first test the demonstrator by only actuating flap. This section describes the tests that were performed.

6.2.1 Shaker tests

The setup of the test with the shaker is shown in figure 6.4a, in this figure, the blue arrow represents the location where the shaker is connected to the demonstrator. Three accelerometers were used to determine the behavior of the blade, see figure 6.4b. The flapping motion was actuated by a shaker that was given a sweep output. The measured response did not give any satisfying data; the response showed many distortion on the curve, see figure 6.5. It turned out that of play occurred in the lag and pitch hinges.

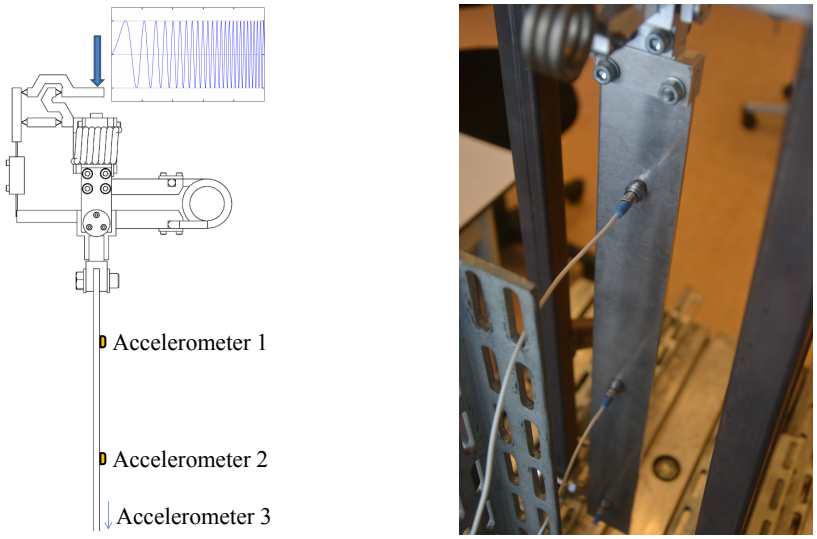

(a) Setup for the demonstrator test (b) Accelerometers at the back of the blade

Figure 6.4: Demonstrator tests

6.2.2 Impact tests

To reduce the effects of the flexible elements between the shaker and the flap hinge, the flexure was uncoupled from the hinge, so that an impact test could be performed. Figure 6.6a shows the test setup with the flexure uncoupled. The blue arrow in this figure indicates the point where the impact was subjected. Again, three accelerometers were located at the back of the blade. Besides uncoupling the shaker from the system, pieces of paper were put between the pitch hinge and the mounting box, see figure 6.6b. This turned out to reduce the play in the pitch hinge significantly.

The FRF of the impact test performed with the blade hanging in the frame is shown as the dashed bold lines in figure 6.5. Although the impact test with the shaker uncoupled gives a smoother response, it does not return the expected mode frequencies. The play in the pitch hinge is reduced significantly, but play still occurred in flapwise direction between the lag shaft and the lag hinge, which could be the reason for not finding the expected mode frequencies.

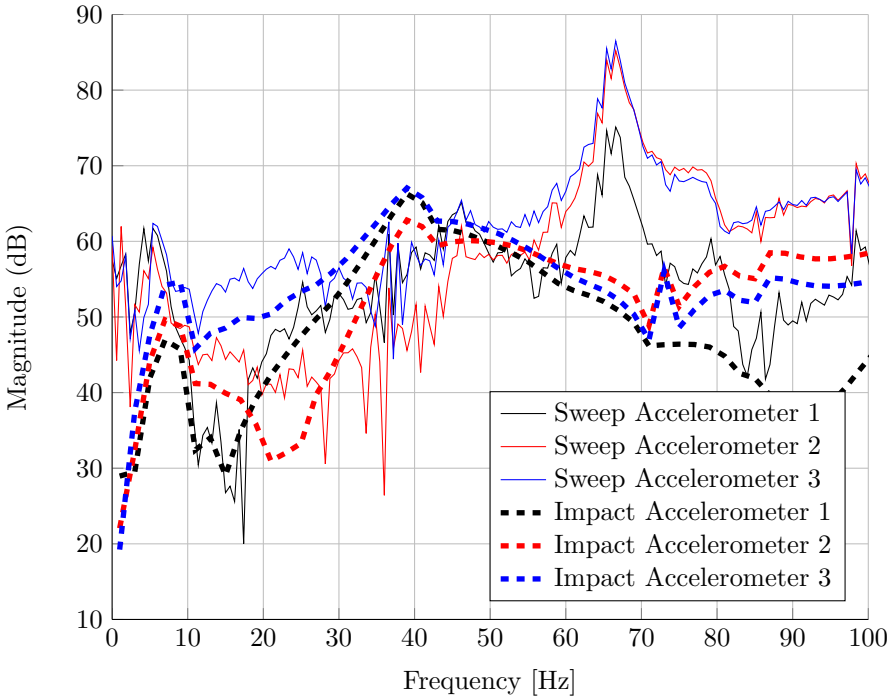

Figure 6.5: FRF of the sweep and impact tests

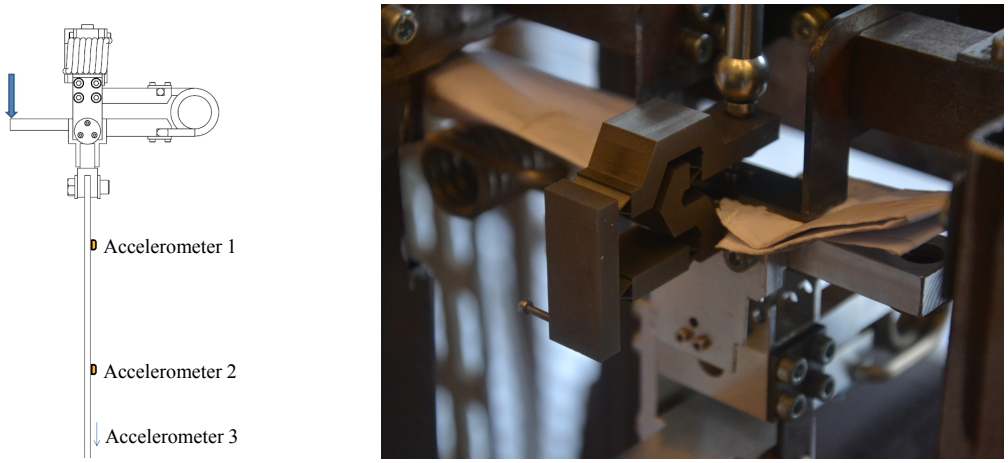

(a) Setup of the impact test

(b) Reduce play in the pitch hinge

Figure 6.6: Impact test of the demonstrator

6.2.3 Lagging test

Because lag was not being activated in the tests described in this section, no effort to measure the rigid lagging frequency was made with these tests. Besides, it was noticed that the blade was not able to display more than one cycle for rigid lagging when an unbalance was brought into the system. The friction that occurred in the connection between the lag and pitch hinges and the torsion spring did not allow the blade to display rigid lagging properly. However, by manually tapping the blade in lagging direction at a frequency of approximately 3Hz, it was observed that the rigid lagging frequency of the demonstrator is around 3Hz, which is the desired frequency.

6.3 Blade tests

Due to the play in the system, the flapping frequencies of the blade could not be determined directly out of the demonstrator. To be able to determine the blade frequencies, the blade and the flap and lag hinge were disassembled from the system to test them individually. As was concluded from the tests with the assembled demonstrator, most of the play occurred on the pitch and lag axes. By disassembling the blade and the flap and lag hinges and testing them separate from the demonstrator, the blade frequencies can be determined without the measurements suffering from the play in the rest of the demonstrator.

A new setup was made for the blade tests. In this new setup, the lag hinge was used to form the connection to the rigid world. The same connection between lag and flap was used for this setup. Two types of tests were performed, the first test was an impact test with only the blade to determine the frequencies of the hanging blade. For the second test, the torsion spring was included. Again, an impact test was performed to determine the effect of the torsion spring on the blade's flapping frequencies.

6.3.1 Pendulum

The first test setup contained no torsion spring, so that the blade frequencies for the pendulum configuration could be measured. The rigid body frequency can be calculated with the standard pendulum formula: $f = \sqrt{\frac{3g}{2L}} = 5.4\text{rad/s} = 0.86\text{Hz}$. As can be seen in figure 6.7, the moment due to gravitational loading depends on θ; it can be considered as a rotational stiffness with a rate of $C_g = \frac{1}{2}mgL$ [Nm/rad]. The first elastic flapping frequency can therefore be calculated using the method of appendix A. This led to an expected frequency of 48.2Hz.

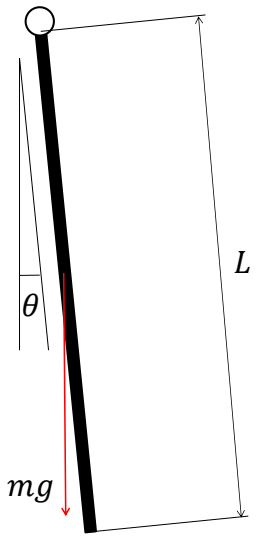

Figure 6.7: Gravitational loading on the blade

After calculating the predicted flapping frequencies, an impact test was performed. The setup for this test is shown in figure 6.8. The red cross in the figure indicates the point of impact, the gray block in the figure represents the connection with the rigid world. As for the tests with the demonstrator, three accelerometers were used to determine the mode frequencies.

Figure 6.9 shows the FRF of the blade for the impact test. As can be seen, an eigen frequency is found at around 48Hz, which was expected. This is the elastic flapping mode. The rigid pendulum mode is not found in this image. This is because the frequency resolution for this measurement was set to 0.5Hz, however, by observing the pendulum frequency when introducing an unbalance in flap, it was concluded that this frequency was in fact around 1Hz.

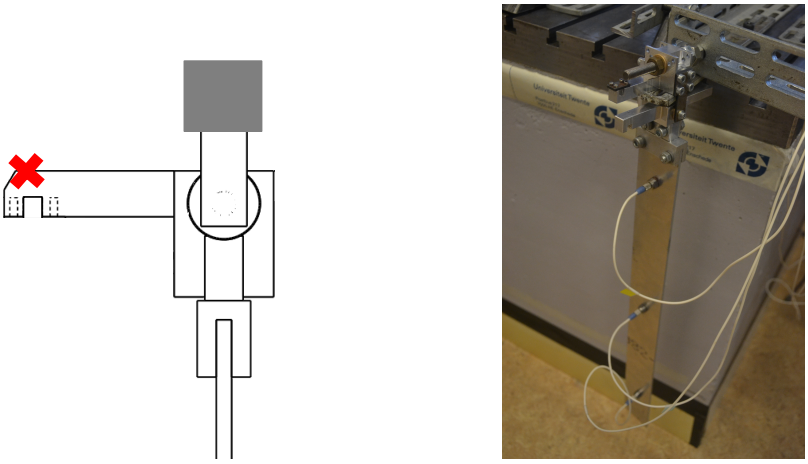

(a) Schematic overview (b) Picture of the setup

Figure 6.8: Pendulum impact test

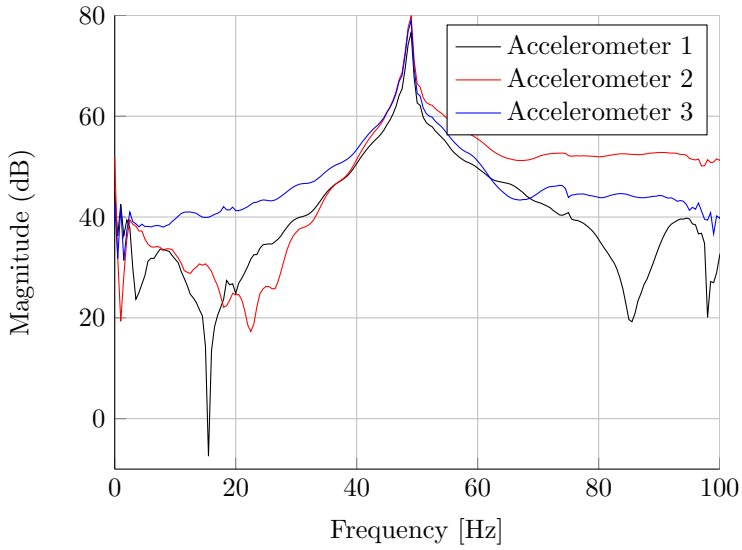

Figure 6.9: FRF of the pendulum system

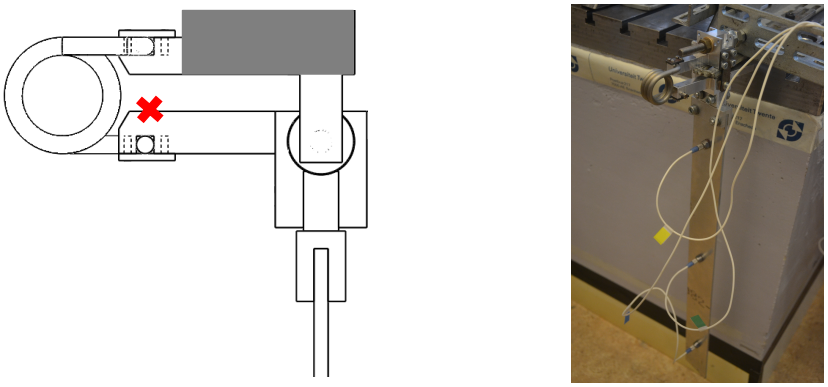

(a) Schematic overview (b) Picture of the setup

Figure 6.10: Impact test with the torsion spring

6.3.2 Torsion spring

The effect of the added torsional stiffness on the mode frequencies was investigated by connecting the torsion spring to the system. Figure 6.10 shows the setup of the impact tests with the torsion spring connected to the system. Again, the red cross indicates the point of impact and the gray block represents the connection with the torsion spring.

The system was designed to display the rigid flapping mode at 10.4Hz and the first elastic flapping mode at 26.8Hz. The impact test will point out if these frequencies are realized in the actual model. The FRF from this test is shown in figure 6.11. As can be seen, two peaks are found up to 40Hz. The first peak is the rigid flapping frequency and is found between 11Hz and 12Hz, while the second peak belongs to the first elastic flapping frequency and is found between 21Hz and 22Hz. These values are not the same as the desired frequencies for which the demonstrator was designed, they are however in the range of these desired frequencies. A possible explanation for the difference between the expected and the measured frequencies is that the rotational stiffness in the hinge might be higher than the stiffness that was used for the calculations. A higher stiffness leads to a higher rigid body frequency, while it will lead to a decrease in the elastic body frequency, as is shown in appendix A.

Appendix B showed that the rotational stiffness in the flap hinge depends on the torsion spring's leg length and its stiffness. The leg length for the flap torsion spring was ordered to be $L_S = 23.5$mm. Remeasuring the leg length showed that this length is somewhere between 21 and 25mm. However, due to the spring wire diameter of $r = 5$mm and the outer spring diameter of 33mm, it is difficult to determine the leg length exactly. If the leg length is assumed to be 22mm, the rotational stiffness in the hinge increases to 2.52Nm/deg instead of the desired 2.2Nm/deg. When a rotational stiffness of 2.52Nm/deg is used for the calculations, this leads to a rigid flapping frequency of $f_{f_r} = 11.1$Hz and a first elastic flapping frequency of $f_{f_{el,1}} = 24$Hz. This shows that a small change in rotational stiffness in the hinge can lead to the shifting of the desired mode frequencies that are in the same order as the measured differences.

6.4 Pitch

After the tests described in the previous section, the blade and the hinges were reassembled in the demonstrator. The final test that was performed for this research included independent actuation of pitch and flap.

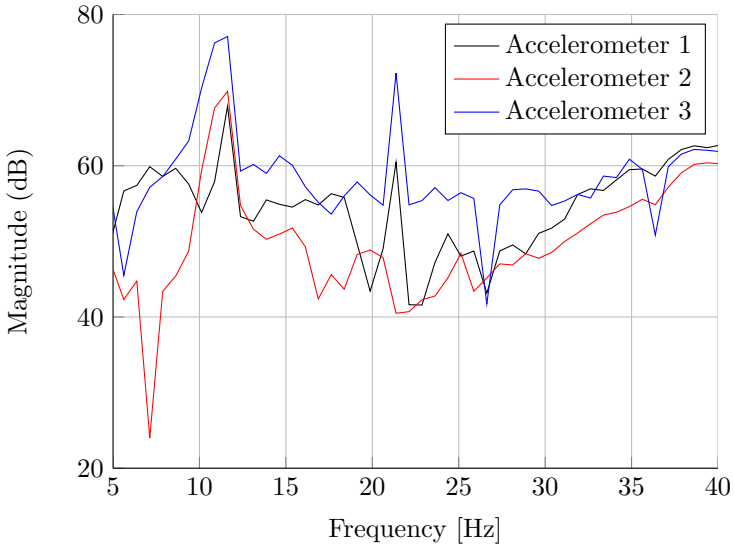

Figure 6.11: FRF of the blade with the torsion spring connected

6.4.1 Test setup

The setup of the demonstrator needed a slight adjustment for this final test. To be able to use the VCM properly, the moving coil of the actuator was connected to an elastic piece of rope, to deliver a counterforce in opposite direction of the magnetic force of the VCM's core, see figure 6.12. This figure shows the top view of the demonstrator. With this elastic, it was possible to locate the VCM in a neutral position. By subjecting an alternating current to the VCM, the pitch is actuated at the frequency of the current. Due to the play that occurred in the experiments with the fully assembled rotor, no effort of monitoring the blade was made for this test. The test was performed to see if problems occur with two independent active actuation sources. Both pitch and flap were actuated for this last test. Pitch was actuated at a constant frequency of 10Hz, while a random noise signal was subjected to the flap hinge.

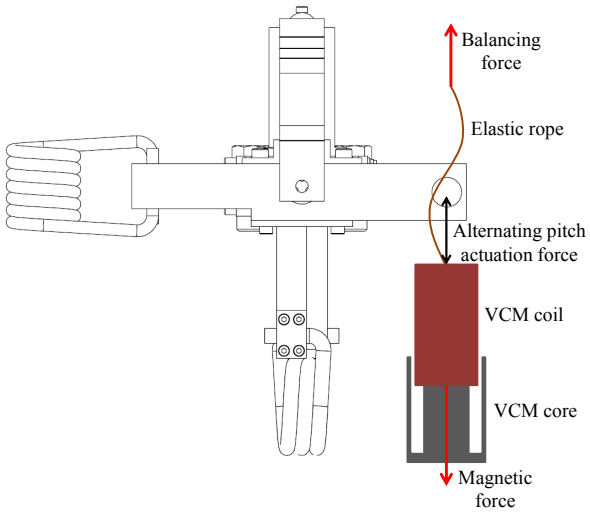

Figure 6.12: Schematic overview of balancing the VCM

6.4.2 Results

Actuation of pitch with the VCM turned out to be difficult; there was no stable neutral position for the VCM. By applying an alternating current on it, cyclic pitch could be simulated. However, when the voltage was increased to generate a larger pitch angle, the coil would quickly be attracted to the permanent magnet of the core, or expelled out of the core.

Besides not being able to find a stable neutral position for the VCM's coil, the fact that the VCM consists of two loose parts turned out to be a problem. The point that is actuated by the VCM will display a pitch angle. Since the coil is able to move inside the core, it will also tend to display slight angle changes. This led to the coil and the core making contact at every cycle, which results in unwanted vibrations in the rest of the system.

6.5 Test conclusions

The final section of this chapter will give the conclusions of the experiments that were performed with the demonstrator.

As was concluded from the analysis of the flexure, the ANSYS model of the mechanism predicted the wrong mode frequencies. The highly overestimated mass of the rigid elements was found to be the cause of this wrong prediction of mode frequencies. Because of this wrong ANSYS analysis, the flexure was found to be more stiff than required and desired.

Due to the amount of play in the lag and pitch hinges, the experiments with the fully assembled demonstrator did not return the expected mode frequencies for flap. For this reason, the blade and flap hinge were tested apart from the system. The impact tests performed did return more satisfying results; the found mode frequencies were in the right range with respect to the expected flapping frequencies. The difference between the measured and the expected frequencies is likely to be caused by the slightly smaller effective leg length of the torsion that is used in the flap hinge. It can however be concluded that the use of external torsion springs in the hinges is a good way to influence the mode frequencies of the blade profile.

After the test with the double excitation of the demonstrator, a normal VCM appeared not to be the best solution for the actuation of pitch directly. Due to the magnetic core of the actuator, no stable neutral position was found. Besides, unwanted vibrations were introduced in the system due to the contact between the coil and the core at every cycle. When monitoring the demonstrator while exciting cyclic pitch, these extra vibrations due to the VCM are highly unfavorable. When for example a guided VCM is used, i.e. a VCM that is guided such that it can only make translating motions, the unwanted vibrations are eliminated from the system.

7. Conclusions & Recommendations

This report described the literature review, the design process and the experiments that were performed with the demonstrator. This final chapter will present the conclusions of the work presented in this thesis. Furthermore, recommendations are given for further research with the demonstrator.

7.1 Conclusions

Two objectives were stated for this research in section 1.2. The conclusions of these objectives are given in this section.

7.1.1 Objective #1

The first objective was stated as follows:

Investigate the added value of on-blade monitoring in RBS by generating an overview of previously performed experiments regarding RBS.

A clear overview of previously performed experimental research regarding RBS was given in section 2.2. This review of experimental research did show some experiments that would have profited if on-blade monitoring would have been an option. Between the reviewed experiments, those that were performed with the main goal to improve maintenance and those that have the goal to get more insight in the behavior of the RBS seem to benefit most by on-blade monitoring.

The reviewed experiments were classified on the basis of the DOFs that were excited and monitored. This classification of experiments was presented in table 2.4 in section 2.3. As was concluded from this table, not many experimental research was performed in which multiple DOFs were being excited and monitored. The setup that is built during this assignment intends to fill a gap in the table.

7.1.2 Objective #2

The second objective was stated as follows:

Design and build a functional setup that represents the behavior of an RBS. This demonstrator is expected to display the different DOFs; flap, lag and feathering.

During this project, a demonstrator was designed, built and tested. An important design requirement was that the lowest natural frequencies of the setup should be related to each other as they are in a real helicopter rotor. The following modes were considered for this: rigid lag, rigid flap and the first elastic flapping mode. The frequencies corresponding to these modes were required to be related to the operation frequency Ω as they are in table 2.1, which shows how the first modes of a fully articulated helicopter rotor are related to Ω. The operation frequency was chosen to be 10Hz. Furthermore, the demonstrator was designed to be actuated by two independent actuation sources. The demonstrator that was built did fulfill many of the design requirements that were listed in section 3.4.

- The demonstrator is able to display the desired DOFs, i.e. flap, lag and rigid feathering.
- The frequencies Ω, f_{f_r} and $f_{f_{el,1}}$ are not exactly related to each other as in table 2.1, the error is around 10% to 20%, which is likely to be caused by a smaller effective leg length of the torsion spring that is used for flap. The rigid lagging frequency f_{l_r} was not measured, since lagging was not actively actuated.
- The demonstrator that was built contains hinges for all DOFs and thus represents a fully articulated helicopter rotor.
- The demonstrator is balanced by gravitational loading. By doing this, no pretension is needed to balance the blade, while a centrifugal force of 1g is simulated by the gravitational loading.
- The flap hinge is designed to clamp a 30x10mm block with a height of 16mm. When blades with a different profile are tested in the demonstrator, a specific blade clamp with a rectangular end block of at least 16mm with a cross section of 30x10mm has to be manufactured. The clamping part should be specific for the blade profile that will be tested.
- Cyclic pitch is actuated by a VCM at a constant frequency of $\Omega = 10$Hz. Actuation of cyclic pitch with a VCM appeared to be less of a good solution than originally thought. Due to the unstable neutral position of the coil, only small voltages could be applied to the actuator. Besides, the fact that the coil made contact with the core at every cycle is highly unfavorable when measurements are performed on the blade.

Referring back to the classification of the reviewed experiments in table 2.4, the demonstrator would be placed in two cells. A new classification table is made with the demonstrator included, see table 7.1. As can be seen, the experiments performed with the demonstrator do not take place in the shaded quarter of the table, i.e. the section where at least two DOFs are excited and actuated. This is because of the amount of play that occurred in the system, which led to the decision to make no attempt of monitoring the DOFs with the fully assembled demonstrator. For future tests, the demonstrator might be placed in the shaded quarter of table 2.4 if the amount of play is reduced. The cell that the demonstrator can be potentially classified to is made black in table 7.1.

For this research, the tests performed were done to conclude on the design of the demonstrator; does it display the modes at the desired frequencies? For this reason, feathering was not monitored; the only interesting mode is the one that is actuated at a known frequency, i.e. cyclic pitch. For lag, the reason not to monitor it was because too much friction occurred between the lag torsion spring and the hinges; the blade was not able to display more than one cycle for rigid lag. However, the rigid lagging frequency was determined to be around the desired 3Hz by manually tapping the blade at approximately 3Hz.

The demonstrator that was built can be used to test different blade profiles. To test a different blade profile, a new part that clamps the blade has to be manufactured. This clamping part is required to have a generic end section, so that it can be mounted in the flap hinge. Besides being able to replace the blade easily, the torsion springs can be replaced as well if a different hinge stiffness is required for a different blade profile.

7.2 Recommendations

This research has delivered a demonstrator that represents a helicopter RBS. This section will describe and motivate the recommendations for further research with the demonstrator. The recommendations will be presented as a list of bullet points, after which they are motivated.

- Redesign of the lag and pitch hinges
  - Reduce play
  - Reduce friction in the connections between the torsion spring and the lag and pitch hinges

Table 7.1: The positions of the demonstrator in table 2.4

		MONITORED DOFS							
		None	**Fe**	**Fl**	**L**	**Fe+Fl**	**Fe+L**	**Fl+L**	**Fe+Fl+L**
EXCITED DOFS	**None**	[15], [23]						[20]	[16]
	Fe					[25]			[17]
	Fl	[26]		[18] **Demo**					
	L	[26]			[24]			[14]	[24]
	Fe+Fl	**Demo**	[19]						Future demo
	Fe+L								
	Fl+L	[27]						[14]	
	Fe+Fl+L								

References

[14] Ormiston
[15] Caradonna
[16] GOAHEAD
[17] NASA '90s
[18] Ozcelik
[19] Büter
[20] Özbek
[23] Monteiro
[24] NASA '80s
[25] Riemenschneider
[26] Bin Yang
[27] Malhotra

Abbreviations

Fe	Feathering
Fl	Flap
L	Lag

- Design for assembly
- Ease the actuation of flap by decreasing the flexure's stiffness
- Select another actuator for actuation of cyclic pitch
- Targeted selection of other torsion springs

Due to the play that occurred in the lag and pitch hinges, it was not possible to determine the mode frequencies of the blade with the fully assembled demonstrator. No noticeable play occurred in the flap hinge with the tests. The reason for this most likely is that the shaft used for the flap hinge is supported by plain bearings at both ends, while the other hinges are supported by only one plain bearing at one end. For future tests with the demonstrator, a redesign of the lag and flap hinge is recommended. For this redesign, it is recommended to use the design of the flap shaft for the structure of the lag and pitch shafts; i.e. use plain bearings at both ends of the shafts. This can lead to an increase in shaft lengths, because two bearings are used for the shafts. Besides reducing play with the new design of the hinges, it is recommended to reduce the friction between the hinges and the lag torsion spring, e.g. by making use of plain bearings in the connections.

For the design of the demonstrator, the focus was on keeping the hinges close to each other and keep the design compact, to place the three axes for the DOFs close to each other. By doing this, the system would represent a helicopter more accurately. Due to the small space between the different parts and subassemblies, assembling the whole system turned out to be a difficult procedure. The amount of space between the pitch hinge, the flexure and the frame resulted in the most problems in the construction phase. If a redesign would be made for the demonstrator, it is recommended to focus more on how to assemble the system. The main focus should still be on keeping the axes of rotation close to each other, however, increasing the space between the flexure, the pitch hinge and the surrounding frame will not

have any effect on the axes of rotation, while having a positive effect on the complexity of the assembly process.

Due to the error with the rigid beam elements in the ANSYS analysis, the modes of the flexure were wrongly predicted. The flexure could have been significantly less stiff, which would have made the actuation of flap more easy. Therefore, it is recommended to reduce the stiffness of the flexure. This can be done by decreasing the width of the hinges of the current flexure. By doing this, the total mass of the system will stay approximately the same, while the leaf bending stiffness will change directly proportional with the hinge width. If the hinge width will be decreased to 5mm instead of 15mm and the bending frequency is estimated by the standard mass-spring formula ($\sqrt{\frac{k}{m}}$), the new bending frequency is calculated to decrease to approximately 56Hz. If the flexure is still judged to be too stiff with this decreased hinge width, it is recommended to make a new design of the flexure. If a new flexure will be designed, the use of ANSYS is still recommended. However, some important adaptations should be made with respect to the model that led to the design of the current flexure. The adaptations that are recommended for the analysis in ANSYS are described in appendix C.3. The recommendations for a new design are given in appendix C.4.

A VCM was selected for the actuation of pitch because it is able to reach high velocities and accelerations without displaying backlash when the direction of the force changes. However, due to the contact between the coil and the core that was made at every cycle, the VCM introduces unwanted vibrations in the system, which is highly unfavorable if the blade is being monitored. For this reason, it is recommended to make some changes for the actuation of pitch. By using a VCM that is guided such that the coil is only able to make translational movements, the contact between the VCM's coil and core will be prevented, while the advantages of the VCM still apply, i.e. the ability to reach high velocities and accelerations without displaying backlash.

If other mode frequencies are desired for a certain blade profile, different torsion springs might be needed. The springs that are used in the current setup are the SF-VFR 8503 and the SF-VFR 8480 [29], both of which the leg length was modified to realize the desired rotational stiffnesses in the hinges. The demonstrator is designed for these specific torsion springs; the distance between the different hinges depends on the spring diameter and the hinges are designed such that the spring wire fits exactly in the extension arms. If different torsion springs are required, it is recommended to search for torsion springs that have the same wire and spring diameter, so that the hinges do not need to be modified and the springs can easily be replaced. The number of coils and the leg length can be modified to change the stiffness of the spring. When a standard torsion spring is selected and the desired rotational stiffness in the hinge is known, the required spring leg length can be calculated according to appendix B. If new torsion springs are ordered, it is recommended to determine the torsional stiffness of it before assembling them in the demonstrator, to be able to predict the mode frequencies with better accuracy.

Bibliography

[1] Department of Defense. Test method standard for enivormental engineering considerations and laboratory tests, 2000.

[2] Civil Aviation Authority. HUMS extension to rotor health monitoring, March 2009.

[3] WiBRATE. Wireless self-powered vibration monitoring and control for complex industrial systems, 2012.

[4] Stefan Oosterik. Towards on-blade monitoring of rotating blade systems: A dynamics based approach. Master's thesis, Universiteit Twente, 2014.

[5] A.R.S. Bramwell, George Done, and David Balmford. *Bramwell's Helicopter Dynamics*. Butterworth-Heinemann, second edition, 2001.

[6] Robert Clark, David Cox, H.C. Curtiss Jr., John W. Edwards, Kenneth C. Hall, David A. Peters, Robert Scanlan, Emil Simiu, Fernando Sisto, and Thomas W. Strganac. *A Modern Course in Aeroelasticity*. Kluwer Academic Publishers, fourth edition, 2004.

[7] John Watkinson. *Art of the Helicopter*. Butterworth-Heinemann, 2003.

[8] Federal Aviation Administration. *Helicopter Flying Handbook*. U.S. Department of Transportation, 2012.

[9] John S. Gero and Udo Kannengiesser. The situated function–behaviour–structure framework, January 2004.

[10] Pieter H. de Jong. *Power Harvesting Using Piezoelectric Materials*. PhD thesis, Universiteit Twente, February 2013.

[11] Scout Helicopter Homepage. Details of MD900.

[12] Burkhard Domke. Aircraft in detail - helicopter rotorhead gallery, 2012.

[13] tech domain.com.

[14] Robert A. Ormiston and William G. Bousman. *A theoretical and experimental investigation of flap-lag stability of hingeless helicopter rotor blades*. Defense Technical Information Center, 1972.

[15] F.X. Caradonna and C. Tung. Experimental and analytical studies of a model helicopter rotor in hover, 1981.

[16] T. Schwarz and K. Pahlke. The GOAHEAD project - overview and selected results, 2010.

[17] W. Keats Wilkie, Paul H. Mirick, and Chester W. Langston. Rotating shake test and modal analysis of a model helicopter rotor blade. Technical report, NASA, 1997.

[18] O. Ozcelik, P.J. Attar, M.C. Altan, and J.W. Johnston. Experimental and numerical characterization of the structural dynamics of flapping beams, October 2013.

[19] Andreas Büter and Elmar Breitbach. Adaptive Blade Twist - calculations and experimental results, 2000.

[20] Muammer Özbek. *Optical Monitoring and Operational Modal Analysis of Large Wind Turbines*. PhD thesis, Technische Universiteit Delft, June 2013.

[21] K. Mulleners, K. Kindler, and M. Raffel. Dynamic stall on a fully equipped helicopter model, 2012.

[22] M. Raffel, F. de Gregorio, W. Sheng, G. Gibertini, A. Seraudi, K. de Groot, and B.G. van der Wall. Generation of an advanced helicopter experimental aerodynamic database, 2009.

[23] João P. Monteiro, Miguel R. Silvestre, Hugh Piggott, and Jorge C. André. Wind tunnel testing of a horizontal axis wind turbine rotor and comparison with simulations from two Blade Element Momentum codes, 2013.

[24] David L. Sharpe. An experimental investigation of the flap-lag-torsion aeroelastic stability of a small-scale hingeless helicopter rotor in hover. Technical report, NASA, 1986.

[25] J. Riemenschneider and S. Opitz. Measurement of twist deflection in active twist rotor, April-May 2011.

[26] Bin Yang and Dongbai Sun. Testing, inspecting and monitoring technologies for ind turbine blades: A survey, 2013.

[27] P Malhotra, R.W. Hyers, J.F. Manwell, and J.G. McGowan. A review and design study of blade testing systems for utility-scale wind turbines, 2012.

[28] Jeffrey D. Singleton and William T. Yeager Jr. Important scaling parameters for testing model-scale helicopter rotors. *Journal of Aircraft*, 37(3), May-June 2000.

[29] Lesjöfors. The spring catalogue #13.

[30] Brammer. Catalogus glijlagers.

[31] Optimum draadvonktechniek. Draadvonken, 2014.

[32] Toon Groen. Personal communication (phone call). EDM manufacterer, Optimum draadvonktechniek, July 2014.

[33] F.C. Campbell. *Manufacturing Technology for Aerospace Structural Materials*, chapter 4. 2007.

[34] Moticont. Linear voice coil motors.

[35] Moticont. Calculation of motor power dissipation for different motion profiles.

[36] KIPP. Axiaal gewricht overeenkomstig din 71802, 2014.

[37] Centerdrill. The flow punch forming process in detail.

[38] ANSYS. *Element Reference*. ANSYS, Inc., November 2009.

[39] Leonard Meirovitch. *Fundamentals of Vibrations*. McGraw-Hill, 2001.

[40] Designerdata. Kruisveerscharnier, 2014.

Appendices

A. Effect of a rotational stiffness

This appendix describes the method that is used to calculate the effect of a rotational stiffness in the flap hinge. An added rotational stiffness is necessary to be able to realize the desired mode frequencies, since the operation frequency Ω is significantly higher than the pendulum frequency of the hanging blade. Because of this added rotational stiffness, the first elastic body frequency will also change. In fact, the 'new' situation is a situation that is between the Clamped-Free beam and the Hinged-Free beam.

The natural bending frequency of a beam is described as follows:

$$\omega_n = A\sqrt{\frac{EI}{mL^3}}, \tag{A.1}$$

where A is a constant that depends on the type of beam configuration. For example, for a beam that is clamped at one end and free at the other end, this constant is $A_C = 3.52$. For a beam that is hinged at one end and free at the other end, this constant becomes $A_H = 15.4$. For the situation with a rotational stiffness at one end and a free other end, this constant depends on the value of the stiffness and will be somewhere between the A_C and A_H. The three different configurations are displayed in figure A.1.

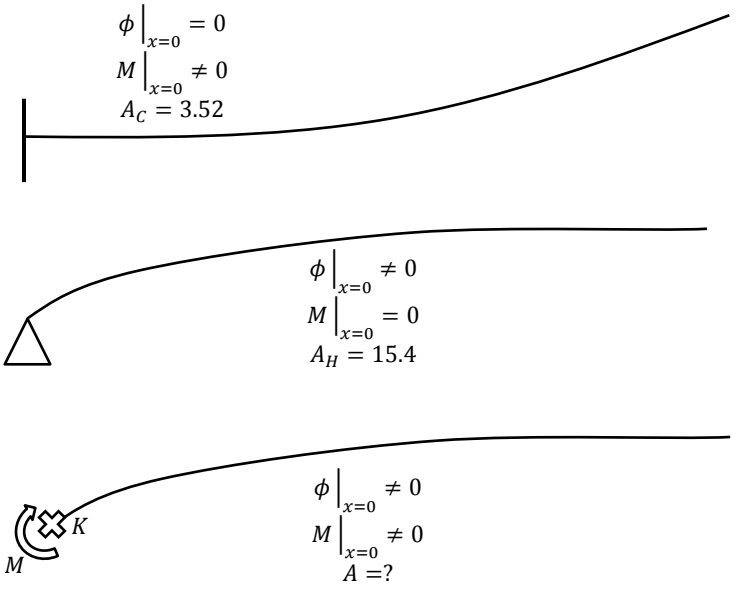

Figure A.1: Elastic body frequencies for different configurations

The partial differential equation of a bending beam is derived in [39]:

$$-\frac{\partial^2}{\partial x^2}\left[EI(x)\frac{\partial^2 y(x,t)}{\partial x^2}\right] + f(x,t) = \rho(x)\frac{\partial^2 y}{\partial t^2}, \qquad 0 < x < L, \tag{A.2}$$

where $f(x,t)$ represents the external forces and $\rho(x)$ is the mass per unit length. For the internal bending frequency, the external forces can be taken as $f(x,t) = 0$. Furthermore, the blade of the demonstrator will have a continuous cross section and mass distribution, so $\rho(x) = \frac{m}{L}$. Equation A.2 can now be rewritten:

$$-EI\frac{\partial^4 y(x,t)}{\partial x^4} = \frac{m}{L}\frac{\partial^2 y}{\partial t^2} \tag{A.3}$$

The solution of this differential equation is assumed to be the product of a function of time and a function of displacement:

$$y(x,t) = Y(x)T(t) \tag{A.4}$$

Substitution of A.4 in A.3 and rewriting results in the following expression:

$$-\frac{EIL}{mY(x)}\frac{d^4Y}{dx^4} = \frac{1}{T(t)}\frac{d^2T}{dt^2} = -\omega^2 \tag{A.5}$$

In this equation, ω is the bending frequency. The solution of the time dependent is as follows:

$$T(t) = A_1 \sin\omega t + A_2 \cos\omega t \tag{A.6}$$

This solution contains two integration constants A_1 and A_2 that are dependent of the initial conditions. The spatial part of equation A.5 is the interesting part, since this is the part where the rotational stiffness has an effect.

$$\frac{d^4Y(x)}{dx^4} - \beta^4 Y(x) = 0, \tag{A.7}$$

where:

$$\beta^4 = \frac{m\omega^2}{EIL} \tag{A.8}$$

The general solution of $Y(x)$ becomes:

$$Y(x) = B_1 \sin\beta x + B_2 \cos\beta x + B_3 \sinh\beta x + B_4 \cosh\beta x \tag{A.9}$$

The constants B_1 to B_4 can be extracted using the boundary conditions of the system. For the blade of the demonstrator, the boundary conditions are as follows:

$$Y(x)|_{x=0} = 0 \tag{A.10a}$$

$$\left.\frac{dY}{dx}\right|_{x=0} = \phi \tag{A.10b}$$

$$EI\left.\frac{d^2Y}{dx^2}\right|_{x=0} + K\phi = 0 \tag{A.10c}$$

$$EI\left.\frac{d^2Y}{dx^2}\right|_{x=L} = 0 \tag{A.10d}$$

$$\left.\frac{d^3Y}{dx^3}\right|_{x=L} = 0 \tag{A.10e}$$

At first, the boundary conditions at $x = 0$, i.e. A.10a, A.10b and A.10c, are filled in:

$$B_2 = -B_4 \tag{A.11}$$

$$B_1 = \frac{\phi}{\beta} - B_3 \tag{A.12}$$

$$-B_2 + B_4 = -\frac{K\phi}{EI\beta^2} \tag{A.13}$$

From A.11 and A.13:

$$B_2 = \frac{K\phi}{2EI\beta^2}, \qquad B_4 = -\frac{K\phi}{2EI\beta^2} \tag{A.14}$$

Substitution A.12 and A.14 in boundary condition A.10d and isolation of B_3 results in the following expression:

$$-\left(\frac{\phi}{\beta} - B_3\right)\sin\beta L - \frac{K\phi}{2EI\beta^2}\cos\beta L + B_3\sinh\beta L - \frac{K\phi}{2EI\beta^2}\cosh\beta L = 0 \tag{A.15}$$

$$B_3 = \frac{\phi}{\beta}\frac{\sin\beta L + \frac{K}{2EI\beta}(\cos\beta L + \cosh\beta L)}{\sin\beta L + \sinh\beta L} \tag{A.16}$$

Substitution of A.12, A.14 and A.16 in boundary condition A.10e:

$$\begin{aligned} &-\left(\frac{\phi}{\beta} - \frac{\phi}{\beta}\frac{\sin\beta L + \frac{K}{2EI\beta}(\cos\beta L + \cosh\beta L)}{\sin\beta L + \sinh\beta L}\right)\cos\beta L + \frac{K\phi}{2EI\beta^2}\sin\beta L \\ &\quad + \frac{\phi}{\beta}\frac{\sin\beta L + \frac{K}{2EI\beta}(\cos\beta L + \cosh\beta L)}{\sin\beta L + \sinh\beta L}\cosh\beta L - \frac{K\phi}{2EI\beta^2}\sinh\beta L = 0 \end{aligned} \tag{A.17}$$

Dividing by $\frac{\phi}{\beta}$ and rewriting results in the following relation:

$$\left(\frac{\sin\beta L + \frac{K}{2EI\beta}(\cos\beta L + \cosh\beta L)}{\sin\beta L + \sinh\beta L}\right)(\cos\beta L + \cosh\beta L) - \cos\beta L = -\frac{K}{2EI\beta}(\sin\beta L - \sinh\beta L) \tag{A.18}$$

Equation A.18 can be solved for β by finding points of intersection. This is done in MATLAB. Now, equation A.8 is considered again:

$$\beta^4 = \frac{m\omega^2}{EIL}$$

The natural frequency ω is the only unknown left in this equation. An expression for ω is found after rewriting the equation:

$$\omega = \sqrt{\frac{\beta^4 EIL}{m}} \tag{A.19}$$

With this method, the bending frequencies can be calculated for a beam that has a rotational stiffness at one side and is free at the other side, which will be the case for the demonstrator.

To control this method, equation A.1 is reconsidered:

$$\omega_n = A\sqrt{\frac{EI}{mL^3}}$$

By combining this equation with the expression of equation A.8, an expression for A can be found:

$$A = \sqrt{\beta^4 L^4} \tag{A.20}$$

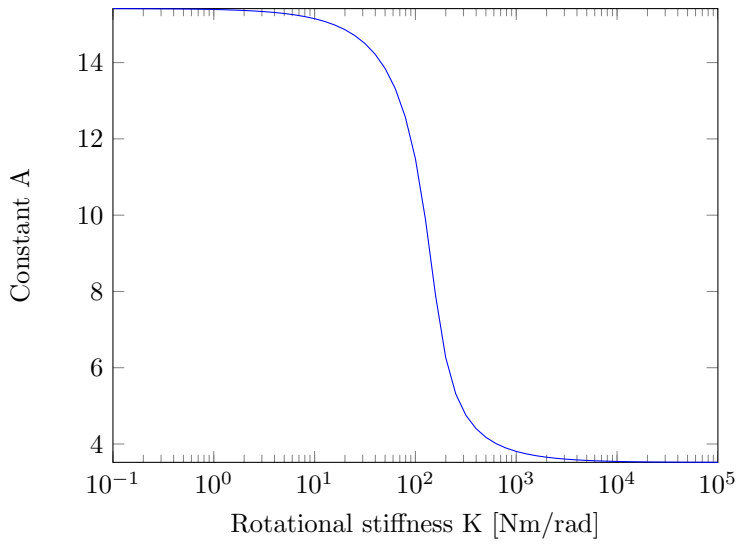

Figure A.2: Relation between constant A and rotational stiffness K

With this expression, the constant A is calculated for varying rotational stiffnesses K. K was varied from 0.1Nm/rad ($\approx$ hinged configuration) to 10^5Nm/rad ($\approx$ clamped configuration). Figure A.2 shows how the factor A changes for varying rotational stiffness K. For $K = 0.1$Nm/rad, A is found to be 15.39, while for $K = 10^5$Nm/rad, A is found to be 3.519. It can be concluded that this method is able to calculate the effect of a rotational stiffness on the elastic body frequencies accurately.

B. External torsion spring design

For the design of the hinges, customized standard torsion springs of the company Lesjöfors were used. To be able to implement the springs externally, the legs of the spring should make an angle of 180° with respect to each other, so that they are pointing in the same direction. As mentioned in chapter 4, the end design was customized. Besides customizing the end design, the leg length had to be determined. Figure B.1 shows the design parameters for the flap hinge that are important to realize the desired torsional stiffness C_F. With the torsion spring constant C_S, the leg length L_S and the arm length L_F of the flap hinge, the rotational stiffness of this hinge can be calculated.

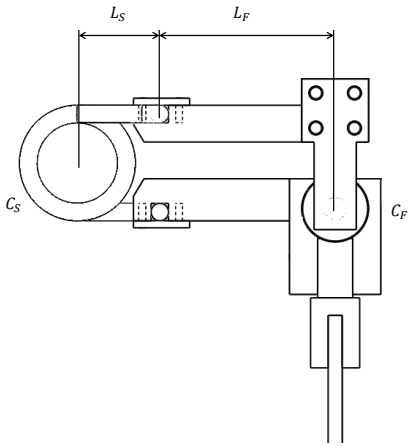

Figure B.1: Parameters for the calculation of the torsional stiffness

If the flap hinge and the blade are rotated over an angle $d\varphi$, the angle change for the spring and the blade are not similar, due to the difference in L_S and L_F. This is schematically shown in figure B.2.

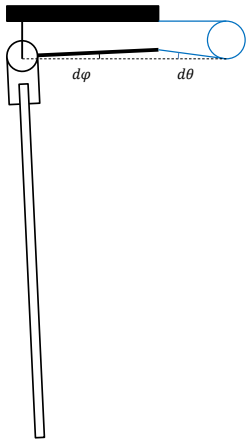

Figure B.2: External torsion spring with a flapping angle

The torsional moment of the spring is calculated as follows: $M_S = d\theta C_S$. This moment is generated by the spring's legs. In case of small angles, the change in distance between the legs ($h_0 - h_1$ in figure B.3) is calculated as follows:

$$dh = d\theta L_S \tag{B.1}$$

Now, the angle change of the flap hinge can be calculated:

$$d\varphi = \frac{dh}{L_F} = \frac{d\theta L_S}{L_F} \tag{B.2}$$

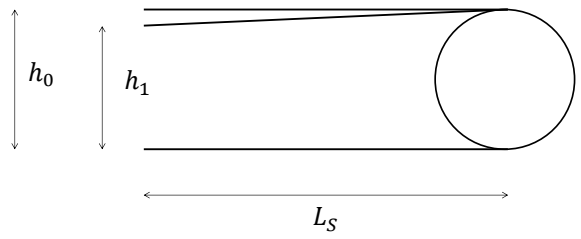

Figure B.3: Torsion spring legs in case of deformation

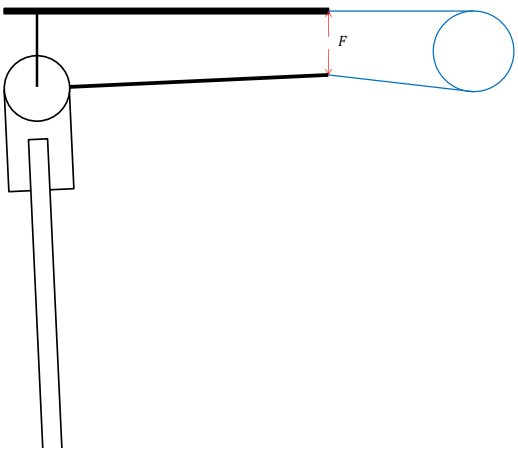

Figure B.4: Force as a result of deformation

The force that the legs of the torsion spring exert on the demonstrator is calculated, after which the resultant moment around the flap axis can be calculated:

$$F = \frac{M_S}{L_S} \tag{B.3}$$

$$M_F = FL_F = \frac{M_S L_F}{L_S} \tag{B.4}$$

Now that the moment and deflection are known, the rotational stiffness that the flap axis experiences can be calculated:

$$C_F = \frac{M_F}{d\varphi} \tag{B.5}$$

Substitution of equations B.2 and B.4 in B.5:

$$C_F = \frac{M_S L_F^2}{d\theta L_S^2} = \frac{C_S L_F^2}{L_S^2} \tag{B.6}$$

This leads to the following expression:

$$\frac{L_F}{L_S} = \sqrt{\frac{C_F}{C_S}} \tag{B.7}$$

With this expression, the required leg length for the selected torsion spring can be calculated. For flap, the required rotational stiffness is calculated to be $C_F \approx 2.2$Nm/deg. A torsion spring with a rate of $C_{S_F} = 0.488$Nm/deg is selected to be used. With a hinge arm of $L_F = 50$mm, the required leg length is calculated to be $L_{S_F} \approx 23.5$mm. For the lag torsion spring, the required stiffness was calculated to be $C_L \approx 0.19$Nm/deg, a spring with a rate of $C_{S_L} = 0.103$Nm/deg was selected and with a hinge arm of $L_L = 50$mm, the required leg length is calculated to be $L_{S_L} = 36.4$mm.

C. ANSYS analysis of the flexure mechanism

The design of the flexure mechanism was described in section 5.1. The flexure was modeled in ANSYS to determine its characteristics, i.e. its stiffness, mode shapes and their corresponding frequencies. This appendix will go into detail on the ANSYS model of the flexure.

C.1 Elements

The finite element simulation software ANSYS APDL was used to investigate the flexure's characteristics and to come up with a suitable design. The model was built up with several different element types. The basis of the structure of the ANSYS model consisted of linear beam elements (BEAM188), these are 3D two node elements. The four hinges were not modeled as beams. Due to the small thickness of the leafs, beam elements are not suitable for modeling of the hinges. The hinges are therefore modeled by four node shell elements (SHELL181). These are better suited for analyzing thin shell structures such as the leafs in the flexure [38].

Introducing shell elements in a structure of beam elements demands some modifications. The flexure was modeled in the xy-plane; the beams were all on modeled on lines in this plane. The shells however should be modeled on areas that are in z-direction. To connect the beam and shell elements, multipoint constraint elements (MPC184) are used. These are elements that can be used to apply constraints between nodes. In this case, they are used as rigid beams to realize a rigid connection between the beams and shells.

To model the effect of the torsional stiffness in the flap hinge of the demonstrator, a COMBIN14 element was used that was modeled as a linear spring. The rotational stiffness K_{flap} is used to calculate the corresponding linear stiffness at the actuation point. The flexure was designed to actuate flap at an arm $x = 50$mm from the flap axis. Since the system will only display small flapping angles, the torsional stiffness at the flap axis can be replaced by a linear stiffness at the point where the flexure will be connected to the flap hinge. By doing this, the effect of K_{flap} can be included without making the model too complex.

In conclusion, the ANSYS model consists out of the following elements: BEAM188, SHELL181, MPC184 and COMBIN14. Figure C.1 shows the ANSYS model with the different elements. As can be seen in this figure, extra beams are modeled where the structure splits. This is better seen in figure C.2. These extra beams are introduced in the model to generate an extra stiffness that is present at these locations; this is the result of the larger thickness of the flexure at the two locations where the structure splits.

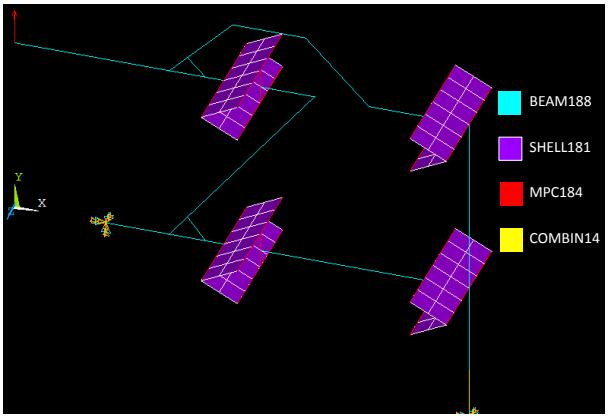

Figure C.1: ANSYS model of the flexure

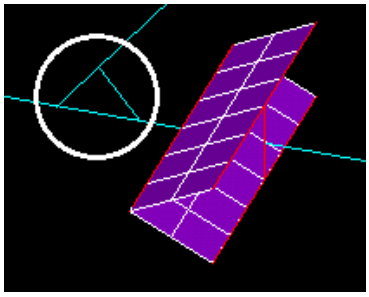

Figure C.2: Extra beam where the model splits

C.2 Verification of the model

To verify the ANSYS model, the stiffness of the flexure is estimated with some hand calculations. The four flexible hinges in the model can be compared to a cross hinge, see figure C.3. The formulas for a cross hinge mechanism [40] are used.

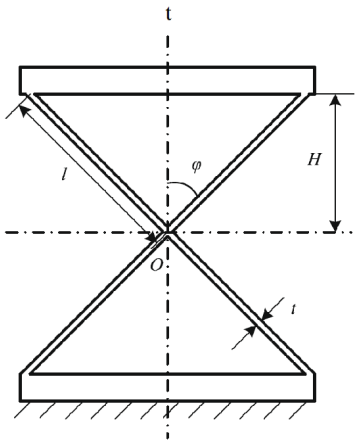

Figure C.3: Cross hinge [40]

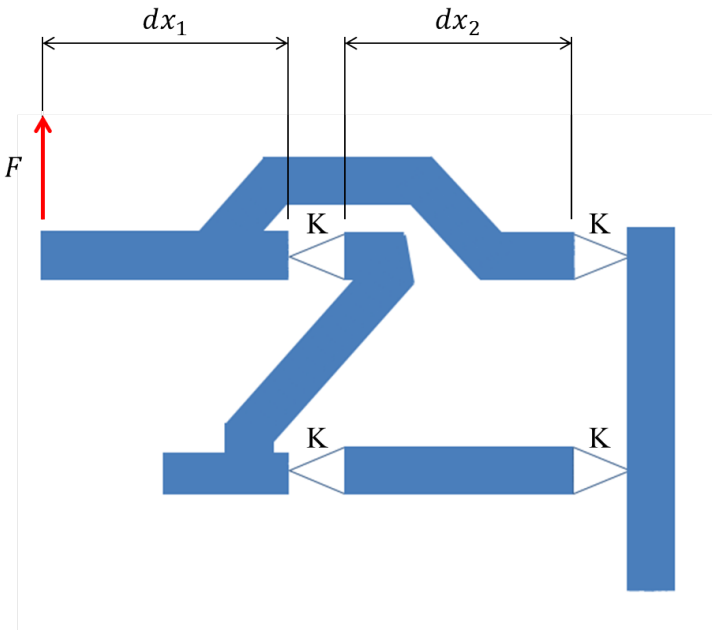

Figure C.4: Structure of the flexure

The stiffness of this cross hinge is calculated as follows:

$$K = \frac{4EI}{H}\cos\varphi = \frac{4EI}{l} \tag{C.1}$$

This stiffness is in Nm/rad. For the designed flexure, the hinges can be considered as half cross springs. The flexible height of a hinge in the flexure is half the flexible height of the cross hinge. The stiffness will therefore be twice as high for a single hinge.

$$K_h = \frac{8EI}{l} \tag{C.2}$$

When the stiffness of the hinges is known, the flexure's stiffness can be estimated. Figure C.4 shows the structure of the flexure. When a force F is applied at distance dx_1 from the first hinge, a moment of Fdx_1 is present at this hinge. Since the hinges move and deform together, a stiffness of $4K_h$ is assumed for the total mechanism. The resulting change in angle θ can now be calculated:

$$\theta = \frac{Fdx_1}{4K_h} \tag{C.3}$$

When the change in angle is known, the vertical displacement of the flexure's end can be estimated. For this estimation, the vertical displacement as a result of the bending leafs of the hinges is neglected. Only the displacement due to rigid rotation of the beams between the hinges is calculated.

$$dy = dx_2 \sin\theta \tag{C.4}$$

Using the same parameters that are used in ANSYS, the stiffness of the flexure can be calculated. For the calculation of the deflection, a force of $F = 10$N is applied.

$$K_h = 2.04\text{Nm/rad} \tag{C.5a}$$

$$\theta = 0.028\text{rad} \tag{C.5b}$$

$$dy = 5.4 * 10^{-4}\text{m} \tag{C.5c}$$

When a static analysis in ANSYS is performed with a force of 10N, the maximum deflection at the flexure's end is $dy = 5.5 * 10^{-4}$m, which is slightly higher than the calculated deflection. It can be concluded that the ANSYS model is reliable.

For this verification, an ANSYS model that only contained the flexure mechanism was used. The modal and static analyses during the design process of the flexure were all performed with a model in which the torsional stiffness of the flap hinge was modeled by a spring element, this was however not done in the analysis that was used for verification of the model. This explains the different values for the deflection of the two models.

C.3 Adaptations after testing

The impact test with the flexure that is described in section 6.1 showed that the ANSYS analysis that was done did not manage to predict the right mode frequencies. The problem turned out to come from the rigid beam elements that were used; the prescribed cross-sectional area of 0.25mm^2 was overwritten to 1m^2. A new analysis where the rigid elements were modeled with low-density material ($\rho = 0.001\text{kg/m}^3$) turned out to predict the first mode frequency better, although still an error of around 30% occurred.

Besides changing the density of the material of the rigid beam elements, decreasing the size of the shell elements also turned out to have a positive effect on the results. This is explained by the fact that more elements are used when the shell element size is reduced, which results in an increase in the number of nodes that are able to deform. Figure C.5 shows two ANSYS models, C.5a is modeled with large shell elements, while C.5b is modeled with small shell elements. Because the leafs are connected to rigid beam elements at both sides, each of the leafs of the model shown in figure C.5a contain only one row of nodes that is able to deform. The number of deformable nodes in figure C.5b increases significantly in each of the leafs. The effect of the rigid beam elements on the behavior of the leafs will therefore be reduced. The difference between the two models is well noticeable; the first mode frequency is 140.8Hz for the model of figure C.5a and 127.5Hz for the model of figure C.5b.

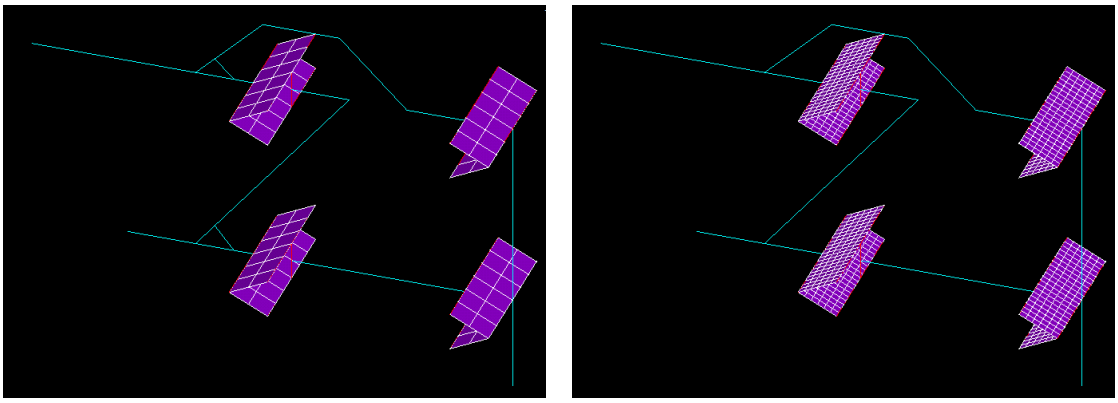

(a) Flexure with large shell elements

(b) Flexure with small shell elements

Figure C.5: ANSYS flexure models

C.4 Recommendations for new flexure design

As was concluded from the tests with the flexure, the mechanism was too stiff to be able to make proper use of the leaf bending mode. The previous section described the adaptations that are recommended to come up with a more accurate analysis in ANSYS. If a new flexure will be designed, it should be designed such that the first mode frequency will decrease. Three recommendations for a new design are given:

- Increase the hinge size
- Decrease the width of the hinges
- Increase mass of the moving beams

The recommendation to increase the hinge size aims at increasing the length of the leafs. As can be seen in the expression for the stiffness of a cross hinge (Equation C.1), an increase of the leaf length leads to an inversely proportional decrease of the hinge stiffness.

When the width of the hinges is decreased, the bending stiffness will decrease with the same proportion as the width. It should be noted that this recommendation aims at changing the width of the hinges only; changing the width of the total flexure will not have any effect, because the mass will change with the same proportion as the width.

The last recommendation given is to increase the mass of the moving beams. If this mass is increased, it will result in a decrease of the first mode frequency. The mass can be increased by increasing the beam height.

A possible new design of the flexure is shown in figure C.6. The numbers in the figure indicate the changes that are made for this design:

1. The hinge width of the two outer hinges is decreased to 5mm. Furthermore, the hinge height and length are both increased with 50%, to increase the leaf length.
2. The width of the two hinges that are closest to the pitch axis are not decreased. If these hinges would also be decreased in width, the complexity of the manufacturing process is likely to increase significantly.
3. The moving beams of the flexure are increased in size, to realize an increase in the mass.
4. The total height of the flexure is increased. This is done with the eye on the recommendation that was given to redesign the pitch hinge and use two plain bearings in this hinge. If this is done, the height of this new hinge will increase, which means that the flexure's height will also need to increase. By doing this, the moving mass of the mechanism will also increase, which is favorable to generate a lower first mode frequency for the mechanism.

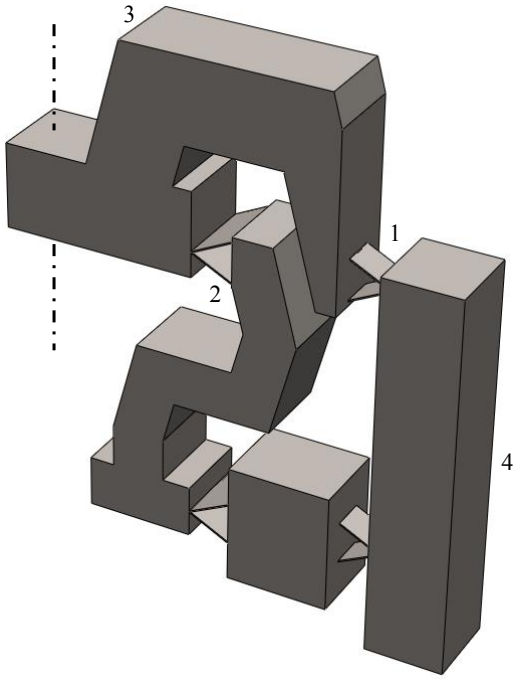

Figure C.6: Possible new design of the flexure

D. Mini-shaker data sheet

PRODUCT DATA

Mini-shaker — Type 4810

USES

- Calibration of accelerometers
- Vibration testing of small objects
- Educational demonstrations
- Mechanical impedance measurements

FEATURES

- Force rating 10 newton (2.25 lbf) sine peak
- Frequency range DC to 18 kHz
- First axial resonance above 18 kHz
- Max. bare table acceleration 550 m/s^2
- Rugged construction
- Optimised to obtain full output force when used with Power Amplifier Type 2718

951138e

Description

Mini-shaker Type 4810 is of the electrodynamic type with a permanent field magnet. It is well-suited as the motive force generator in mechanical impedance measurements where only smaller forces are required. It can also be used in the calibration of vibration transducers, both to determine their sensitivity, by comparison with a standard accelerometer, as well as their frequency response, up to 18 kHz.

The suspension system consists of radial flexure springs that restrict the moving element to almost perfectly rectilinear motion. Laminated flexure springs provide a high degree of damping to minimise distortion due to flexure resonances.

The object to be vibrated is attached to the table by means of a 10 – 32 UNF screw, the thread size commonly used for mounting accelerometers. Performance limits defined by the maximum displacement (6 mm), maximum force (10 N or 7 N depending on frequency), and the first axial resonance of the moving element (above 18 kHz), are shown in Fig. 1.

Fig. 1
Sine performance curves for Type 4810

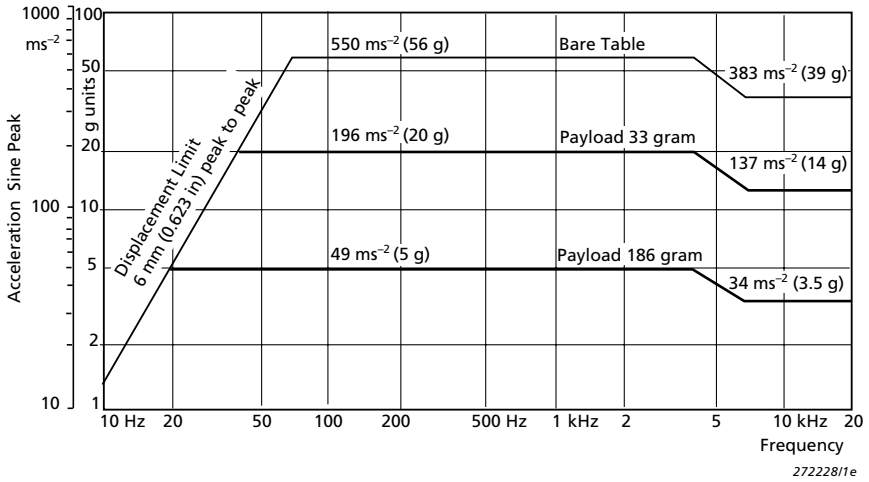

Specifications – Mini-shaker Type 4810

COMPLIANCE WITH STANDARDS

CE compliance with EMC Directive

compliance with EMC Requirements of Australia and New Zealand

Safety, EMC Emission and Immunity: According to relevant standards: EN 61010–1, IEC 61010–1, UL 3111–1, EN 50081–1/2, IEC 61000–6–1/2/3/4, EN 61326–1, CISPR22 Class B limits, FCC Rules Part 15, EN 50082–1/2, EN 61326–1
Temperature: According to IEC 60068–2–1 & IEC 60068–2–2
Operating temperature: +5 to +40°C (41 to 104°F)
Storage temperature: –25 to +70°C (–13 to 158°F)
Humidity: According to IEC 60068–2–3, Damp Heat: 90% RH (non-condensing at 40°C (104°F))
Mechanical: Non-operating according to IEC 60068–2–6, IEC 60068–2–27, IEC 60068–2–29

SPECIFICATIONS
FREQUENCY RANGE: DC to 18 kHz

FIRST MAJOR ARMATURE RESONANCE: Above 18 kHz

FORCE RATING (PEAK):
10 N (2.25 lbf). 65 Hz to 4 kHz
7 N (1.5 lbf). 65 Hz to 18 kHz

MAX. BARE TABLE ACCELERATION (PEAK):
550 m/s^2 (65 Hz to 4 kHz)
383 m/s^2 (6.5 kHz to 18 kHz)
(1 m/s^2 = 0.102 g)

MAX. DISPLACEMENT (PEAK-TO-PEAK): 6 mm (0.236 in)

DYNAMIC FLEXURE STIFFNESS: 2 N/mm (11.5 lb./in)

DYNAMIC WEIGHT OF THE MOVING SYSTEM: 18 grams

MAGNETIC FIELD: Permanent magnet

MAX. INPUT CURRENT: 1.8 A RMS

COIL IMPEDANCE: 3.5 Ω at 500 Hz

CONNECTION: Microsocket 10–32 UNF

TABLE SIZE: 14 mm (0.55 in) diameter

FASTENING THREAD: 10–32 UNF

WEIGHT: 1.1 kg (2.4 lb)

DIMENSIONS
Diameter: 76 mm (3 in)
Height: 75 mm (2.9 in)

Ordering Information

Type 4810	Mini-shaker
Includes the following accessories:	
AO 0069	Cable for connection of Type 4810 to Power Amplifier Type 2718
YQ 2962	Threaded Steel Stud, 0.3 in 10–32 UNF

Optional Accessories

EE 0112	ENDEVCO 2311-1 ISOTRON® Force Transducer
EE 0113	ENDEVCO 2311-10 ISOTRON Force Transducer
EE 0114	ENDEVCO 2311-100 ISOTRON Force Transducer
EE 0115	ENDEVCO 2311-500 ISOTRON Force Transducer
EE 0357	ENDEVCO Model 2312 Force Transducer
Type 8203	Force Transducer/Impact Hammer
UA 0125	Mounting Equipment (includes isolated studs YP 0150 and non-isolated studs YQ 2960)
WA 0429	Trunnion
WZ 0066	Nylon Stinger Kit
EE 5227-002	Bushing Adaptor, ¼–28 UNF to 10–32 UNF
EE 5004	Adaptor, Male 10–32 UNF to Male ¼–28 UNF
JP 0150	Adaptor, 4 mm Socket Pair to BNC Plug for use with old Type 2706

BP 0232 – 14 01/08

HEADQUARTERS: DK-2850 Nærum · Denmark · Telephone: +4545800500 · Fax: +4545801405 · http://www.bksv.com · e-mail: info@bksv.com
Australia (02)9450-2066 · Austria 0043-1-8657400 · Brazil (011)5182-8166 · Canada (514)695-8225 · China (86) 1068029906
Czech Republic 02-67021100 · Finland (0)9-755 950 · France (01)69907100 · Germany 06103/733 5-0 · Hong Kong 25487486 · Hungary (1)2158305
Ireland (01)803 7600 · Italy 02 57 68061 · Japan 03-3779-8671 · Republic of Korea (02)3473-0605 · Netherlands (31)318 559290 · Norway 66771155
Poland (22)858 9392 · Portugal (1)4711453 · Singapore (65) 377-4512 · Slovak Republic 421 2 5443 0701 · Spain (91)6590820 · Sweden (08)4498600
Switzerland (0)1 880 70 35 · Taiwan (02)7139303 · United Kingdom (0) 1438 739 000 · USA 800 332 2040
Local representatives and service organisations worldwide

E. AVM 30-15 Data sheet

Model	Units	AVM 30-15
Stroke	mm	15
Force sensitivity (at mid stroke)	N/A	7.35
Back EMF constant	V/m/s	7.35
Continuous force (at 100 °C)*	N	4.63
Continuous force (at 155 °C)*	N	5.88
Peak force	N	29.4
Resistance	ohms	10.6
Inductance	mH	2.94
Recommended bus voltage	V	48.0
Voltage at peak force	V	42.4
Continuous current (coil at 100 °C)*	A	0.63
Continuous current (coil at 155 °C)*	A	0.80
Peak current	A	4.0
Actuator constant	N/SqRt(W)	2.26
Electrical time constant	ms	0.3
Mechanical time constant	ms	4.7
Clearance of coil	mm	0.60
Power at peak force	W	169.6
Max coil temperature	°C	155.0
Coil assembly mass	g	24.1
Core assembly mass	g	92.7

* Continuous force measured without any additional mounting plate or heat sink on coil.

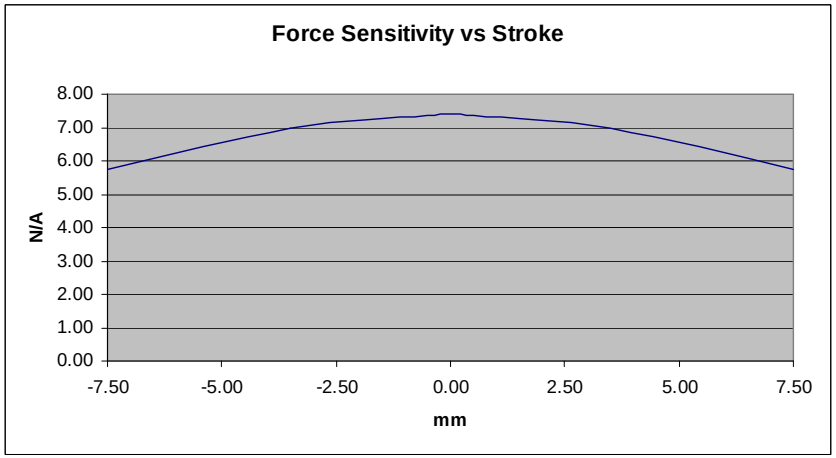

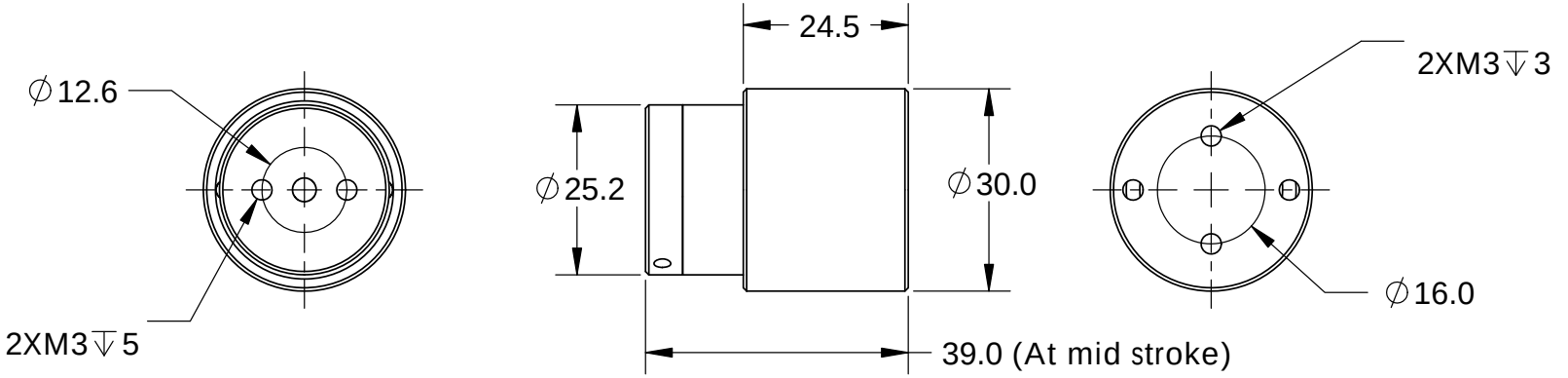

Stroke = +/- 7.5 mm (total 15 mm)

REVISION: 3 rd angle projection Dimensions in mm .X +/- 0.05 X +/- 0.5	TITLE: AVM30-15	
MATERIAL:	DWG NO.	A4
DATE 12 Sept 2005	SCALE:1:5	SHEET 1 OF 1